

Diabetes Mellitus–Induced Long Noncoding RNA *Dnm3os* Regulates Macrophage Functions and Inflammation via Nuclear Mechanisms

Sadhan Das,* Marpadga A. Reddy,* Parijat Senapati, Kenneth Stapleton, Linda Lanting, Mei Wang, Vishnu Amaram, Rituparna Ganguly, Lingxiao Zhang, Sridevi Devaraj, Dustin E. Schones, Rama Natarajan

Objective—Macrophages play key roles in inflammation and diabetic vascular complications. Emerging evidence implicates long noncoding RNAs in inflammation, but their role in macrophage dysfunction associated with inflammatory diabetic complications is unclear and was therefore investigated in this study.

Approach and Results—RNA-sequencing and real-time quantitative PCR demonstrated that a long noncoding RNA *Dnm3os* (dynamin 3 opposite strand) is upregulated in bone marrow-derived macrophages from type 2 diabetic db/db mice, diet-induced insulin-resistant mice, and diabetic ApoE^{-/-} mice, as well as in monocytes from type 2 diabetic patients relative to controls. Diabetic conditions (high glucose and palmitic acid) induced *Dnm3os* in mouse and human macrophages. Promoter reporter analysis and chromatin immunoprecipitation assays demonstrated that diabetic conditions induce *Dnm3os* via NF-κB activation. RNA fluorescence in situ hybridization and real-time quantitative PCRs of subcellular fractions demonstrated nuclear localization and chromatin enrichment of *Dnm3os* in macrophages. Stable overexpression of *Dnm3os* in macrophages altered global histone modifications and upregulated inflammation and immune response genes and phagocytosis. Conversely, RNAi-mediated knockdown of *Dnm3os* attenuated these responses. RNA pull-down assays with macrophage nuclear lysates identified nucleolin and ILF-2 (interleukin enhancer-binding factor 2) as protein binding partners of *Dnm3os*, which was further confirmed by RNA fluorescence in situ hybridization immunofluorescence. Furthermore, nucleolin levels were decreased in diabetic conditions, and its knockdown enhanced *Dnm3os*-induced inflammatory gene expression and histone H3K9-acetylation at their promoters.

Conclusions—These results demonstrate novel mechanisms involving upregulation of long noncoding RNA *Dnm3os*, disruption of its interaction with nucleolin, and epigenetic modifications at target genes that promote macrophage inflammatory phenotype in diabetes mellitus. The data could lead to long noncoding RNA-based therapies for inflammatory diabetes mellitus complications.

Visual Overview—An online [visual overview](#) is available for this article. (*Arterioscler Thromb Vasc Biol.* 2018;38:1806-1820. DOI: 10.1161/ATVBAHA.117.310663.)

Key Words: atherosclerosis ■ chromatin ■ inflammation ■ lncRNA ■ macrophages ■ phagocytosis

Metabolic syndrome and diabetes mellitus are associated with insulin resistance, hyperglycemia, and hyperlipidemia that contribute to chronic inflammation implicated in the pathogenesis of vascular complications such as atherosclerosis.¹⁻³ Monocyte recruitment into target tissues and differentiation into macrophages are key processes in inflammation associated with such complications. Diabetes mellitus accelerates these vascular complications by skewing monocyte/macrophage polarization, proliferation and dysfunction to enhance inflammation, foam cell formation, and promote defective apoptosis and efferocytosis.²⁻⁵ These adverse pro-inflammatory effects of diabetes mellitus and insulin resistance on macrophages can be mediated by high glucose (HG),

advanced glycation end products, elevated free fatty acids such as palmitic acid (PA) and oxidized lipids.^{2,3,6,7} Several studies demonstrated the role of oxidative stress, activation of the receptor for advanced glycation end products, signaling pathways including protein kinase C, and transcription factors (TF) such as NF-κB.^{8,9} Epigenetic mechanisms, including promoter histone H3 lysine 9/14 acetylation (H3K9ac) and H3K4 methylation have also been implicated in inflammatory gene regulation associated with diabetic complications.¹⁰ However, much less is known about the role of noncoding RNAs like long noncoding RNAs (lncRNAs) in regulating genes and processes associated with inflammation and macrophage dysfunction in diabetes mellitus.

Received on: December 19, 2017; final version accepted on: June 6, 2018.

From the Department of Diabetes Complications and Metabolism, Beckman Research Institute of City of Hope, Duarte, CA (S. Das, M.A.R., P.S., K.S., L.L., M.W., V.A., R.G., L.Z., D.E.S., R.N.); and Department of Pathology and Immunology, Texas Children's Hospital, Houston (S. Devaraj).

*These authors contributed equally to this article.

The online-only Data Supplement is available with this article at <https://www.ahajournals.org/journal/atvb/doi/suppl/10.1161/atvbaha.118.310663>.

Correspondence to Rama Natarajan, PhD, Department of Diabetes Complications and Metabolism, Beckman Research Institute of City of Hope, 1500 E Duarte Rd, Duarte, CA 91010. E-mail natarajan@coh.org

© 2018 American Heart Association, Inc.

Arterioscler Thromb Vasc Biol is available at <https://www.ahajournals.org/journal/atvb>

DOI: 10.1161/ATVBAHA.117.310663

Nonstandard Abbreviations and Acronyms

BMDMs	bone marrow-derived macrophages
ChIP	chromatin immunoprecipitation
Dnm3os	dynamin 3 opposite strand
EV	empty vector
HG	high glucose
ILF-2	interleukin enhancer-binding factor 2
LDL	low-density lipoprotein
lncRNA	long noncoding RNA
PA	palmitic acid
PMs	peritoneal macrophages
RT-qPCR	real-time quantitative PCR
SNE	soluble nuclear supernatant
SSC	saline-sodium citrate
STZ	streptozotocin
T2D	type 2 diabetes mellitus
TF	transcription factor
TNF	tumor necrosis factor
TPM	transcripts per million

Emerging evidence shows lncRNAs are involved in diverse biological processes such as cell proliferation and differentiation.^{11,12} lncRNAs are longer than 200 bp, lack coding potential and are expressed from intergenic regions or introns, as antisense to coding transcripts, pseudogenes, host genes of microRNAs, and from enhancers.^{11–14} lncRNA actions include transcription regulation via directing epigenetic factors such as polycomb repressive complexes to chromatin, acting as scaffolds for chromatin remodeling proteins and TFs and regulation of mRNA stability/translation, and inhibition of microRNA functions.^{11–13,15} Changes in lncRNA expression can dysregulate key functions of cardiac, vascular, and renal cells implicated in diabetic vascular complications and cardiovascular diseases.^{14,16–19} Recent studies have identified several lncRNAs expressed in macrophages and monocytes that mediate pro- and anti-inflammatory processes, cell differentiation, and survival.²⁰ These macrophage lncRNAs act through diverse mechanisms including regulation of proinflammatory TFs like NF- κ B, interaction with hnRNPs (heterogeneous nuclear ribonucleo proteins) and epigenetic regulators such as polycomb repressive complexes to promote chromatin remodeling at target gene promoters.^{20–23} However, these aspects of lncRNA functions have not been studied in diabetes mellitus-induced macrophage dysfunction.

We recently demonstrated that bone marrow-derived macrophages (BMDMs) obtained from obese, type 2 diabetic (T2D) db/db mice exhibited enhanced inflammatory genes, and dysregulation of genes associated with macrophage alternate activation compared with BMDMs from control nondiabetic db/+ mice. Interestingly, these transcriptome changes were also associated with altered expression of several lncRNAs. One of the upregulated lncRNAs, *E330013P06* was found to promote proinflammatory and proatherogenic phenotype in macrophages.²⁴ However, the regulation and function of other differentially expressed lncRNAs in diabetic macrophages are not known. Here, we demonstrate that a lncRNA *Dnm3os* (dynamin 3 opposite strand) is upregulated in macrophages and monocytes

under diabetic conditions via NF- κ B activation. Furthermore, we found *Dnm3os* interacts with nucleolin, a nuclear protein, in macrophages, and that disruption of *Dnm3os*-nucleolin interactions under diabetic conditions can enhance inflammatory gene expression via epigenetic mechanisms. The results illustrate novel mechanisms underlying lncRNA-dependent regulation of macrophage inflammation in diabetes mellitus.

Materials and Methods

The authors declare that all supporting data are available within the article (and its online supplementary files).

Isolation of BMDMs and Peritoneal Macrophages From Mice

Animal experiments were performed in accordance with protocols approved by the Institutional Animal Care and Use Committee. BMDMs were prepared from 10 to 12-week-old T2D male and female db/db mice and control db/+ littermates, and male C57BL/6 mice (Jackson Laboratories, Maine) as described.²⁴ Bone marrow cells were obtained from femurs and tibia and differentiated into macrophages for 7 to 8 days in macrophage complete medium containing DMEM (Cat. No. 12-707F, Lonza, Basel, Switzerland) with 5.5 mmol/L glucose, 10% heat inactivated fetal bovine serum (Cat. No. S11150, Atlanta Biologicals, Flowery Branch, GA), 2 mmol/L glutamine, penicillin/streptomycin (100 μ mol/L), 50 μ mol/L β -mercaptoethanol, and 10 mmol/L HEPES, pH 7.4 supplemented with 20 ng/mL of M-CSF (Cat. No. 416-ML-050, R&D Systems, Minneapolis, MN). Thioglycollate-elicited peritoneal macrophages (PMs) were isolated from control C57BL/6 and streptozotocin (STZ) injected (50 mg/kg per day for 5 days) type 1 diabetic mice as well as C57BL/6 mice (8 weeks old) fed high-fat diet (60% kcal, Research Diets Inc, D12492i) or normal chow diet for 8 weeks as described.²⁴ In addition, male *Apoe*^{-/-} mice (Jackson Laboratory, stock number 002052) were injected with STZ (50 mg/kg per day) or citrate buffer for 5 consecutive days. BMDMs were prepared at 20 weeks postdiabetes mellitus (>500 mg/dL of glucose versus 160 mg/dL in controls) when diabetic *Apoe*^{-/-} mice exhibited accelerated atherosclerosis. Mouse macrophage cell line RAW264.7 (ATCC, Manassas, VA) was maintained in macrophage complete medium. Where indicated, macrophages were treated with media containing 200 μ mol/L PA (Nu-Check Prep, Inc, MN) or control BSA for indicated periods. PA stock solutions (10 mmol/L) were freshly prepared in BSA, diluted to the indicated concentration in macrophage complete medium, incubated for 30 minutes at 37°C, and filtered with 0.2 μ m filter before treating macrophages and monocytes.²⁴

Isolation of Primary Human Monocytes and Human Macrophages

Human monocyte experiments were performed in accordance with approved protocols from the Baylor College of Medicine and the City of Hope Medical Center. After informed consent CD14+ monocytes were obtained from T2D patients and healthy controls (age and sex matched) at the Baylor College of Medicine. Patient data and monocyte isolation methods have been described.²⁴ In some experiments, CD14+ monocytes from healthy donors (All Cells, Emeryville, CA) and THP1 monocytes (ATCC TIB-202) were differentiated into macrophages using MCSF (50 ng/mL) for 1 week and PMA (20 ng/mL, up to 48 hours), respectively.

RNA Isolation and Gene Expression

Total RNA was isolated using RNeasy mini kit (Cat. No. 74106, Qiagen, Valencia, CA), with on-column digestion with DNase I digestion (Cat. No. 79254, Qiagen). Total RNA (0.2–1 μ g) was used to synthesize cDNA using the Prime Script RT Master Mix (Cat. No. RR036A, Takara, Mountain View, CA) for coding genes, QuantiTect Reverse Transcription Kit (Qiagen) or High-Capacity cDNA Reverse Transcription kit (Cat. No. 4368814, Thermo Fisher Scientific) for

lncRNAs, and qScript microRNA cDNA Synthesis Kit (Quanta Bio, Beverly, MA) for miRNAs. Gene expression was analyzed by quantitative PCR (qPCR) using SYBR Green reagent and TaqMan assays (Cat. No. 4367659 and 7352042, respectively, Applied Biosystems, Foster City, CA) with gene-specific primers (Table II in the [online-only Data Supplement](#)), and PerfeCTa SYBR Green SuperMix (Quantabio) for miRNAs in triplicate on 7500 Fast Real-Time PCR system (Applied Biosystems). Relative gene expression between control and treated groups were determined using $2^{-\Delta\Delta C_t}$ method^{24,25} after normalization with *Ppia*, *18S*, *HPRT1*, and *Rplp0* (for coding genes and lncRNAs) and *U6* (for miRNAs).

Transfection of Macrophages

RAW macrophages were transfected with indicated siRNAs, expression vectors or promoter reporter plasmids using Nucleofection kit (Lonza, Gaithersburg, MD) for macrophages (program Y-001)^{24,25} or RNAiMAX (Cat. No. 13778-150, Thermo Fisher Scientific) according to manufacturer's protocols. THP1 macrophages were transfected with indicated GapmeRs (50 nmol/L) using RNAiMAX. Transfected cells were processed for RNA extraction, phagocytosis assays, luciferase assays, and chromatin immunoprecipitation (ChIP) assays as indicated at 48 to 72 hours posttransfection.

RAW Macrophage Cell Lines Stably Overexpressing *Dnm3os*

We generated *Dnm3os* expression vector (pDnm3os) by cloning *Dnm3os* (7.928 kb) into pcDNA 3.1 (+) (Thermo Fisher) and verified by DNA sequencing. RAW264.7 macrophages were transfected with pDnm3os or pcDNA3.1(+) empty vector (EV) using nucleofection. Single cells clones stably expressing *Dnm3os* (RAW-Dnm3os) and EV (RAW-EV) were selected by Geneticin (Cat. No. 10131027, Thermo Fisher Scientific, 500 μ g/mL).

Cloning of *Dnm3os* Promoter and Luciferase Assays

Mouse genomic DNA fragments (1250 and 731 bp containing *Dnm3os* promoter (-1000 and -500 bp upstream from TSS) were cloned into SacI-XhoI sites of the pGL4.10[luc2] (Promega, Madison, WI) upstream of firefly luciferase and verified by DNA sequencing. RAW264.7 cells were cotransfected with *Dnm3os* reporters and pRL-TK expressing Renilla luciferase (internal control) using nucleofection. Next day treated \pm PA (6 hours) or HG (24 hours). Luciferase activity in cell lysates measured with Dual-Luciferase Reporter Assays (Cat. No. E1910, Promega). In some experiments, reporter plasmids were cotransfected with p65 (NF- κ B) expression vector.

In Vitro Transcription/Translation Assay

We determined coding potential of *Dnm3os* using T7 TNT quick coupled transcription/translation system (Promega, Madison, WI, Cat. No. L1170) and transcend colorimetric nonradioactive translation detection system (Promega, Cat. No. L5070) following manufacturer's instructions.

Dnm3os and Nucleolin Knockdown Using siRNAs and GapmeRs

RAW264.7 cells and BMDMs from db/+ and db/db were transfected with siRNAs (20 nmol/L) targeting mouse *Dnm3os* (siDnm3os; Cat. No. R-173881-00-0005, GE-Dharmacon, Lafayette, CO) or control siNTC oligos (Cat. No. D-001810-10-05, GE-Dharmacon) for 48 hours. To knockdown nucleolin, RAW-EV and RAW-Dnm3os cell lines were transfected with Dicer-substrate siRNAs (20 nmol/L) targeting nucleolin (Cat. No. DsiNA-NCL3 is mm.i.Ncl.13.3) and control NC1 oligos (from Integrated DNA Technologies, Skokie, Illinois) with RNAiMAX for 72 hours. Then treated \pm PA and processed for RNA isolation and ChIP assays. THP1 macrophages were transfected with antisense LNA-modified GapmeR targeting human *DNM3OS* (Cat No./ID: LG00201301-DDA, Qiagen) and a control antisense

LNA GapmeR (negative control-A, Cat No. LG00000002, Qiagen) for 48 hours to knockdown *DNM3OS*.

Phagocytosis Assays

RAW macrophages, BMDMs, or THP1 macrophages were transfected with siRNAs or indicated expression vectors and 48 hours later plated on either coverslips in 24 well plates for microscopy or in black 96 well plates to measure fluorescence. Mouse macrophages were incubated with FITC-labeled *E. coli* BioParticles from Vybrant Phagocytosis Assay Kit (Thermo Fischer Scientific) for 2 hours at 37°C, washed twice with PBS, and incubated with Trypan blue to quench fluorescence from external *E. coli* bioparticles. Cells were fixed with paraformaldehyde (15 minutes) and washed with PBS. Cells on coverslips were mounted on slides using Vectashield containing DAPI and images collected using EVOS fluorescence microscope. Numbers of macrophages displaying phagocytosis were counted using Photoshop and results reported as % of phagocytosed cells (FITC relative to total by DAPI stain). When cells were plated in 96 wells, fluorescence from phagocytosed *E. coli* bioparticles was read on Infinite 200 Pro 96 well fluorescent plate reader (Tecan) at 483/518 nm. Results were reported as arbitrary fluorescence units or fold over control cells. Phagocytosis assays in THP1 macrophages were performed in 96 wells by incubating with pHrodo Green *E. coli* BioParticles Conjugate for Phagocytosis (Cat. No. P35366, Thermo Fisher Scientific) for 2 hours. Fluorescence from internalized particles was determined using Infinite 200 Pro (500/538 nm) and results expressed as % of Control GapmeR transfected cells.

Subcellular Fractionation of Macrophages

RNA from nuclear and cytoplasmic fractions of RAW macrophages and db/db mice BMDMs were prepared using Nuclear and cytoplasmic RNA purification kit (Cat. No. 21000, Norgen, ON, Canada) following manufacturer's protocols. Chromatin from RAW macrophages was isolated following published methods.²⁶ RAW264.7 cells (80% confluent) were detached by Accutase and 2×10^7 cells were lysed with equal volumes of Buffer A (10 mmol/L HEPES pH 7.5, 10 mmol/L KCl, 10% glycerol, 340 mmol/L sucrose, 4 mmol/L MgCl₂, 1 mmol/L DTT, and 1x Complete protease inhibitor (Cat. No. 11697498001, Sigma) containing 0.2% Triton X-100 (12 minutes on ice). Lysates were centrifuged at 1200g, 5 minutes, 4°C, and supernatants were saved as cytoplasmic fractions. The nuclear pellets were washed once (500g for 5 minutes at 4°C) with 250 μ L of NRB (20 mmol/L HEPES pH 7.5, 50% Glycerol, 75 mmol/L NaCl, 1 mmol/L DTT, and 1x Complete protease inhibitor), resuspended in 250 μ L NRB and mixed with an equal volume of NUN buffer (20 mmol/L HEPES, 300 mmol/L NaCl, 1 mol/L Urea, 1% NP40, 10 mmol/L MgCl₂, and 1 mmol/L DTT). After incubation for 5 minutes on ice, centrifuged (1200g, 5 minutes, 4°C) and soluble nuclear supernatant (SNE) was transferred to another tube. The depleted nuclear pellet was washed once with 1 mL buffer A and chromatin-enriched pellet was resuspended in 50 μ L buffer A. RNA was isolated from SNE and chromatin-enriched fractions using Trizol (Cat. No. 15596026, Thermo Fisher Scientific) and RNeasy mini kit.

Western Blotting

Whole cell protein lysates and Western blotting were performed as described.²⁷ Western blots were probed with indicated primary antibodies for 24 hours at 4°C, washed, and incubated with HRP-conjugated anti-rabbit (Cat. No. AP307P, Millipore, Darmstadt, Germany, 0.33 μ g/mL) or antimouse (Cat. No. 1706516, Biorad Hercules, CA, 0.07 μ g/mL) secondary antibodies for 1 hour at room temperature. Blots were washed and protein bands visualized using chemiluminescence detection. Antibodies against Histone H3 (ab1791), H3K27ac (ab4729), H3K9ac (ab4441), and nucleolin (ab22758) were from Abcam, Cambridge, United Kingdom. Histone antibodies were used at 1 μ g/mL and nucleolin at 0.5 μ g/mL. As for loading controls, blots were probed with actin (A5441, Sigma-Aldrich, 0.33 μ g/mL) or tubulin (sc-5286, Santa Cruz Biotechnology Inc, Dallas, TX, 1 μ g/mL) antibodies.

ELISA

Cell culture supernatants from mouse macrophages transfected with *Dnm3os* siRNAs (siDnm3os) or control siRNAs (siNTC) were centrifuged at 200g for 10 minutes to remove cell debris and stored frozen at -80°C until assayed using ELISA kits for the cytokines IL-6 (Cat. No. 550950, Lot no. 726959, BD Bioscience, La Jolla, CA) and TNF (tumor necrosis factor)- α (Cat. No. MTA00B, Lot No. P161075, Minneapolis, MN) according to the manufacturer's protocols. Results were expressed as pg/mL.

ChIP Assays

ChIP assays were performed as described.^{28,29} Briefly, RAW macrophages were crosslinked with 1% formaldehyde (Cat. No. F8775, Sigma-Aldrich) for 10 minutes at room temperature, quenched with 0.125 mol/L glycine for 5 minutes, and washed with ice-cold PBS. Cells were lysed in ChIP lysis buffer and chromatin was sheared (up to 200–600 bp) by sonication (8 cycles, 30 sec on / 30 sec off) using Bioruptor Pico (Diagenode, Denville, NJ). Immunoprecipitation was performed using 3 μg of antibodies specific to H3K9ac (Cat. Nos. ab10812, lot No. GR143846-2; Abcam, Cambridge, United Kingdom), or control rabbit IgG, overnight at 4°C . Immune complexes were collected onto 25 μL of magnetic protein G Dynabeads (Cat. No. 10003D, Novex, Waltham, MA) and washed. ChIP DNA was purified and dissolved in MilliQ water. ChIP assays for TF p65 (NF- κB) were performed using nuclear lysates prepared from cross-linked RAW macrophages.³⁰ Cells were lysed in cold lysis buffer 1 (140 mmol/L NaCl, 1 mmol/L EDTA, 50 mmol/L HEPES pH 7.5, 10% glycerol, 0.5% NP40, 0.25% Triton-x-100, 1x protease inhibitor) for 10 minutes at 4°C . Lysates were centrifuged at 2000 rpm for 5 minutes and the nuclear pellet was resuspended in lysis buffer 2 (10 mmol/L Tris pH 8.0, 200 mmol/L NaCl, 1 mmol/L EDTA, 0.5 mmol/L EDTA, 0.5 mmol/L EGTA, and 1x protease inhibitor), incubated for 10 minutes at 4°C and centrifuged at 2000 rpm for 5 minutes. The chromatin pellet was resuspended in ChIP lysis buffer, sonicated and ChIP assays were performed using 5 μg of p65 specific antibody (F-6 antibody, Cat. Nos. Sc-8008x, lot No. A1817; Santa Cruz Biotechnology, Inc. Dallas, TX). ChIP DNA in technical triplicates was analyzed by qPCR using SYBR Green reagent on the 7500 Fast Real-Time PCR system using ChIP-qPCR primers (Table II in the [online-only Data Supplement](#)). ChIP enrichment relative to input (% input) was calculated using the formula $2^{-(\text{Ct}_{\text{ChIP}} - \text{Ct}_{100\% \text{input}})}$.

RNA Fluorescence In Situ Hybridization to Determine Subcellular Localization of *Dnm3os*

RAW macrophages and indicated BMDMs were plated on coverslips and RNA fluorescence in situ hybridization was performed using 5'-end labeled (FAM) LNA oligonucleotide probes targeting *Dnm3os* (Sequence-attggacgagagcgtctgtga, Exiqon, Valencia, CA). Hybridization was performed as described.³¹ Cells were blocked by incubating in prehybridization buffer (3% bovine serum albumin and 4x saline-sodium citrate buffer [SSC]) for 1 hour at room temperature. Hybridization was performed with prewarmed hybridization mix (10x dextran sulfate and 4xSSC) containing 25 nmol/L LNA-FAM probe, at 50°C (20°C – 25°C below the predicted probe T_m) for 1 hour with gentle agitation. Then cells were washed with 4xSSC containing 0.1% Tween-20 3x and once each with 2xSSC, 1xSSC, and PBS for 5 minutes each at room temperature. Cells were blocked with 1% BSA for 45 minutes at 4°C and incubated with primary anti-nucleolin antibody (Cat. Nos. ab22758, lot No. GR258417-1; Abcam, 1 $\mu\text{g}/\text{mL}$) or anti-ILF-2 (interleukin enhancer-binding factor 2; Cat. Nos. ab28772, lot No. GR178687-8; Abcam, diluted 10 $\mu\text{g}/\text{mL}$ with 0.1% BSA) for 30 minutes at room temperature. Cells were washed 3x with PBS, 5 minutes each, and incubated with appropriate Alexa Fluor-conjugated secondary antibody (1:400 dilution in 0.1% BSA, Cat No. NEF710001EA, lot No. 2031274; Perkin Elmer, Boston, MA) for 30 minutes at room temperature. After washing cells with PBS, nuclei were stained with 1 $\mu\text{g}/\text{mL}$ 4',6'-diamidino-2-phenylindole (DAPI; Cat. No. D1306, Invitrogen by Thermo Fisher Scientific) and mounted in ProLong Gold antifade reagent (Cat. No. P36930,

Thermo Fisher Scientific). The images were acquired in an LSM 10 Meta Confocal microscope (Carl Zeiss) and analyzed by the software provided by Carl Zeiss and Image J software.

Dnm3os RNA Pull-Down and Mass Spectrometry Analysis

RNA pull-down was performed as described before with some modifications.³² Briefly, full-length *Dnm3os* sense and antisense strands were Biotin-labeled by in vitro transcription using Biotin RNA labeling Mix (Cat No. 11685597910, Roche) and T7 RNA Polymerase (Cat No. EP011, Stratagene). Biotinylated *Dnm3os* sense and antisense RNAs were treated with RNase-free DNase I and purified on G-50 Sephadex Quick Spin columns (Cat No. 11274015001, Roche). Biotinylation efficiency for sense and antisense strands were determined by Biotin Chromogenic Detection Kit (Cat No. K0661, Thermo Scientific). Biotinylated RNA (1 μg) was denatured by heating to 60°C for 10 minutes and slow-cooled to 4°C . RNA was mixed with 1 mg of nuclear extract prepared from PMs (for mass spectrometry) and RAW macrophages (for Western blot validations) in RNA immunoprecipitation buffer (150 mmol/L KCl, 25 mmol/L Tris pH 7.4, 0.5 mmol/L DTT, 0.5% NP40, 100 mmol/L PMSF, and 1x protease inhibitor) and incubated at 4°C for 2 hours. Then, 60 μL of Streptavidin agarose beads (Cat No. SA10004, Invitrogen) were added to each binding reaction and further incubated at 4°C for 2 hours. Beads were quickly washed 5x in Handee spin columns (Cat No. 69725 Pierce, Thermo Fisher Scientific). Proteins were eluted using SDS buffer, separated on a 4% to 15% precast SDS gel (Cat No. 5671084, Criterion, Biorad, Hercules, CA) and stained with SimplyBlue SafeStain (Cat No. LC6065, Life Technologies). Bands were excised and subjected to protein identification by City of Hope's Mass Spectrometry Core. In some experiments, eluted proteins were also analyzed by Western blotting with indicated antibodies.

Gel-separated proteins were reduced with DTT (Cat No. R0861, Thermo Fisher Scientific), alkylated with iodoacetamide (Cat No. A3221-10VL, Sigma-Aldrich), and digested with a mixture of trypsin and LysC (Promega, Madison, WI). Peptides were extracted from the gel, evaporated to dryness in a vacuum centrifuge, and resuspended in 0.1% formic acid. Digested peptides were analyzed by LC/MS using an Orbitrap Fusion Mass Spectrometer with an EasyNano1000 nano-flow UHPLC (both Thermo Fisher Scientific). Peptides were loaded onto a 75 $\mu\text{m} \times 2 \text{ cm}$ PepMap trapping column packed with 3 μm C_{18} silica particles, 100 \AA pore size, then eluted through a 75 $\mu\text{m} \times 25 \text{ cm}$ PepMap analytical column packed with 2 μm C_{18} silica particles, 100 \AA pore size (both Thermo Fisher Scientific) using a 85-minute linear buffer A/B gradient from 8% to 25% buffer B (buffer A: 0.1% aqueous formic acid, buffer B: 0.1% formic acid in acetonitrile). MS Spectra of the intact peptides were acquired in the Orbitrap, and CID MS/MS spectra were acquired in the ion trap. Data were searched using Sequest in Proteome Discoverer 2.1 (Thermo Fisher Scientific). The database used was a concatenation of the *Mus musculus* RefSeq proteome and a database of common laboratory contaminant proteins and was searched separately in the forward (target) and reverse (decoy) direction. The search assumed tryptic specificity with a maximum of 2 missed cleavages, a precursor ion tolerance of 5 ppm, and a fragmentation ion tolerance of 0.6 Da. It assumed quantitative carbamidomethylation of cysteine and potential oxidation of methionine and acetylation of the protein amino terminus. Search results were loaded into Scaffold version 4.8.4 for probability assignment.

RNA-Seq and Ribosome Profiling Data Analysis

RNA-seq was performed at City of Hope's Integrative Genomics Core on HiSeq 2500 platform (Illumina, San Diego, CA). Raw sequences (Table I in the [online-only Data Supplement](#)) were aligned to the mouse reference genome mm9 using TopHat v2.0,³³ and the expression levels of RefSeq genes were counted using customized R scripts. The counts were normalized by trimmed mean of M value method and differentially expressed genes between groups were identified using Bioconductor package edgeR (fold change >1.5 and $P < 0.01$).³⁴ Additionally, DESeq2 package³⁵ was used to normalize

counts and identify differentially expressed genes (log₂ fold change ≥ 0.5 and *P*adj < 0.1). Differential genes identified using both methods were used to determine significantly modulated gene ontology and pathways using DAVID online annotation tools³⁶ and gene set enrichment analysis.³⁷ Enriched gene sets were represented in a bubble plot using plotly package in R. Briefly, expression values (transcripts per million [TPM]) in RAW-EV and RAW-*Dnm3os* (overexpressed) data sets were calculated for genes in enriched gene sets and used to make the bubble plot with the size of the bubble representing the number of genes. Log₂ fold change and $-\log_{10}$ *P* values of each gene were used to make a volcano plot using R scripts and differentially regulated genes are shown in green. Circos plot was generated using Circos software³⁸ with differentially regulated genes represented on mm9 chromosomes with links drawn from *Dnm3os* genomic location to the other genes. Only genes identified in the enriched gene sets from gene set enrichment analysis are shown on the Circos plot. Motif analysis of differentially expressed gene promoters was performed using TRAP (<http://trap.molgen.mpg.de/cgi-bin/home.cgi>).³⁹

Ribosome profiling data (GSE100739) and corresponding RNA-seq data (GSE100873) were downloaded from Gene Expression Omnibus database. Sequences were aligned to mm9 as above using TopHat, and expression levels were expressed as TPM. Ribosomal occupancy was calculated for selected RNA and expressed as the ratio of ribosomal profiling TPM to input RNA-seq TPM as described.⁴⁰

Data Deposition

RNAseq data is deposited in the Gene Expression Omnibus database (accession number GSE107557).

Statistical Analysis

Values are expressed as mean+SEM. GraphPad Prism 7.02 software (GraphPad Prism Software Inc, San Diego, CA) was used for statistical analyses. Normal distribution of each sample group was confirmed by Shapiro-Wilk normality test before comparing groups. For statistical comparison of 2 groups, unpaired 2-tailed Student *t* test was used. For the comparison of 3 or more groups with similar variances, 1-way ANOVA followed by Tukey or Dunnett post hoc tests were used. *P* values < 0.05 were considered statistically significant for all tests used.

Results

Macrophage *Dnm3os* Is Upregulated in Diabetes Mellitus

We previously reported that several lncRNAs were differentially expressed in BMDMs from T2D db/db mice compared with control nondiabetic db/+ mice, but the function of only one of them (*E330013P06*) was determined.²⁴ Here, we investigated the regulation and functional role of another lncRNA *Dnm3os*, which was highly upregulated in BMDMs from db/db mice compared with db/+ (Figure 1A). *Dnm3os* is expressed as a 7.928 kb long transcript containing a single exon on mouse chromosome 1 from the opposite strand of a coding gene dynamin 3 (*Dnm3*), and its function in macrophages is unknown. To investigate *Dnm3os* functions, we first validated its upregulation using real-time quantitative PCR (RT-qPCR) in BMDMs from db/db macrophages compared with the control db/+ (Figure 1B). However, levels of the coding gene (*Dnm3*) on the opposite strand were not altered (results not shown). Next, we examined *Dnm3os* expression in other mouse models of metabolic syndrome and diabetes mellitus. Results showed that *Dnm3os* expression is also increased in PMs from high-fat diet-induced insulin-resistant mice versus normal chow diet fed mice (Figure 1C), PMs from

STZ-induced type 1 diabetic mice (Figure 1D), and BMDMs from STZ-induced diabetic ApoE^{-/-} mice (Figure 1E) that depict accelerated atherosclerosis⁴¹ versus respective controls. Thus, *Dnm3os* upregulation may play a role in macrophage dysfunction associated with diabetes mellitus, insulin resistance, and macrovascular complications. A human ortholog, *DNM3OS* is also located on human chromosome 1 and shares 83% homology with mouse *Dnm3os*. We found that *DNM3OS* expression is significantly increased in CD14⁺ monocytes from T2D patients versus healthy controls (Figure 1F) demonstrating human disease relevance.

Nuclear Localization and Chromatin Enrichment of *Dnm3os*

Because lncRNA functions are dependent on subcellular localization,¹⁵ we first examined *Dnm3os* levels in nuclear and cytoplasmic fractions in mouse RAW 264.7 macrophages. Results showed that *Dnm3os* is highly enriched in nuclear fractions compared with cytoplasmic (Figure 1G). Nuclear RNAs *U6* snRNA and *Neat1* served as controls (Figure 1H and 1I). As nuclear lncRNAs may interact with chromatin to regulate gene transcription, we examined *Dnm3os* levels in chromatin and SNE from RAW macrophages. Results showed that *Dnm3os* is enriched by 2-fold in the chromatin fraction compared with SNE (Figure 1J). The known chromatin-associated lncRNA *Kcnq10t1*²⁶ served as positive control (Figure 1K). *Ppia* (loading control) showed similar *Ct* values in both chromatin and SNE fractions (Figure 1L). RNA fluorescence in situ hybridization further confirmed nuclear localization of *Dnm3os* and also showed that its levels increased in RAW cells treated with PA (200 μ mol/L, 24 hours), a free fatty acid elevated in diabetes mellitus (Figure 1M). Furthermore, *Dnm3os* was also localized in the nucleus in BMDMs from db/db and db/+ mice and its signal was clearly increased in db/db BMDMs versus db/+ cells (Figure 1N). Similar nuclear enrichment and PA-mediated upregulation were also observed in National Institutes of Health 3T3 fibroblasts (Figure 1 in the [online-only Data Supplement](#)). These results suggest that *Dnm3os* may have nuclear functions to modulate gene expression in macrophages.

Dnm3os Is Regulated by NF- κ B Under Diabetic Conditions

We next examined the mechanism of *Dnm3os* upregulation under diabetic conditions using BMDMs treated with PA, normal glucose and HG. *Dnm3os* was significantly induced by PA with peak expression at 3 hours compared with control (Figure 2A), and by HG at 24 hours in BMDMs (Figure 2B). Moreover, PA also induced *DNM3OS* in human THP1 derived macrophages as well as in human primary CD14⁺ monocyte-derived macrophages from multiple donors (Figure 2C and 2D), confirming similar regulation in human macrophages. To investigate TFs regulating *Dnm3os* expression, we used TRANSFAC and Consite databases⁴² to identify putative promoter TF binding sites. Results revealed an NF- κ B binding site at -490 to -481 bp upstream of *Dnm3os* transcription start site. To verify the role of NF- κ B, we generated 2 reporter constructs by cloning wild-type *Dnm3os* promoter (-1000 to

Dnm3os upregulates in DM

Dnm3os upregulates in BMDMs from DM mice

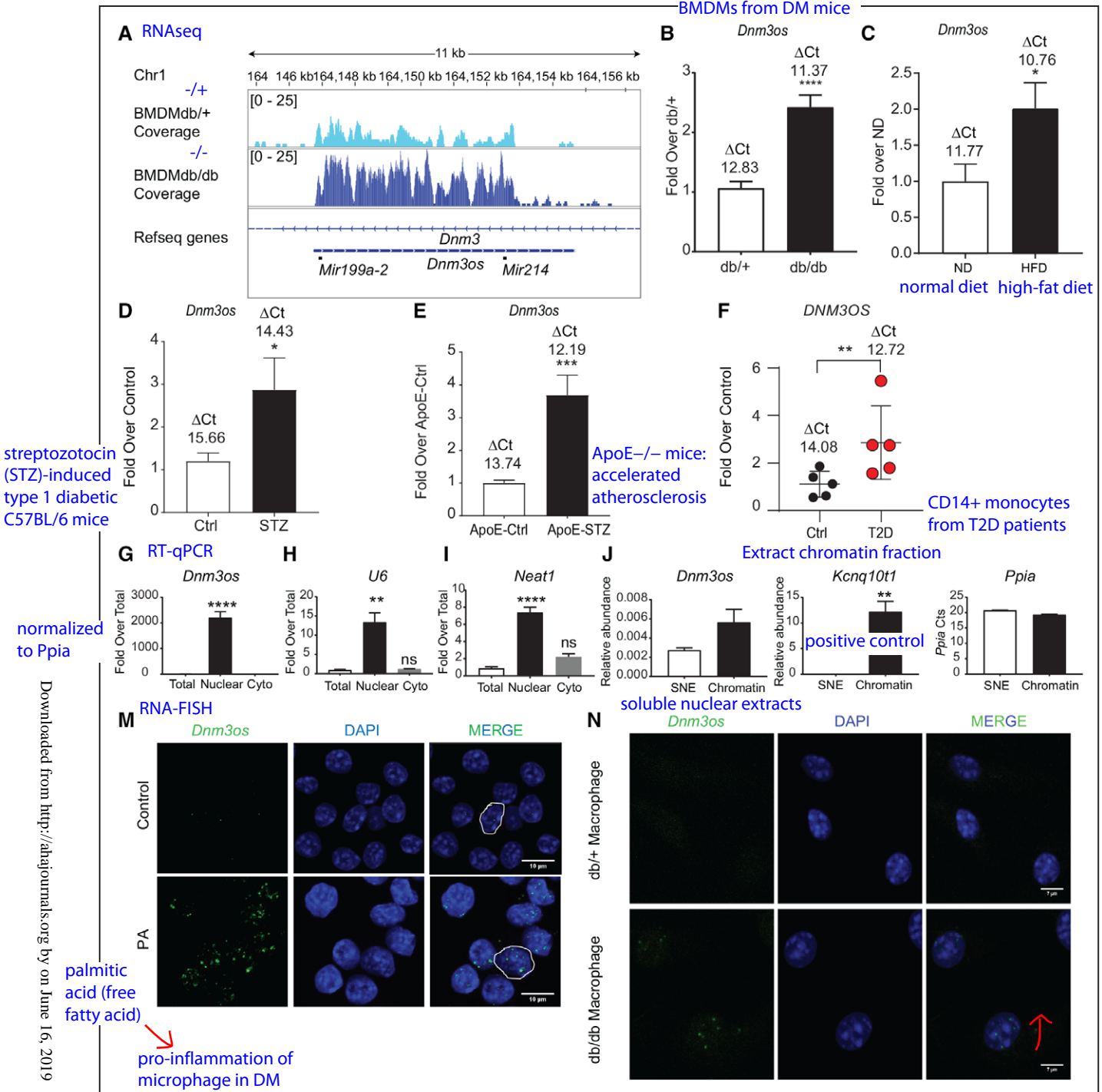


Figure 1. *Dnm3os* (dynamin 3 opposite strand) is upregulated in macrophages in diabetes mellitus and enriched in nucleus. **A**, Normalized profiles of RNA-seq signals for long noncoding RNA (lncRNA) *Dnm3os* in macrophages. Each data track shown is on the same scale for bone marrow-derived macrophages (BMDMs) from control db/+ and type 2 diabetic (T2D) db/db mice. **B**, Real-time quantitative PCR (RT-qPCR) validation of increased *Dnm3os* expression in BMDMs from db/db vs db/+ mice; **(C)** peritoneal macrophages (PMs) from high-fat diet (HFD) fed C57BL/6 mice vs normal diet (ND) mice; **(D)** control (Ctrl) and streptozotocin (STZ)-induced type 1 diabetic C57BL/6 mice (T1D); **(E)** BMDMs from control ApoE^{-/-} mice (ApoE-Ctrl) and STZ-injected ApoE^{-/-} (ApoE-STZ) mice; and **(F)** CD14⁺ monocytes from control (Ctrl) and T2D patients. Gene expression normalized to reference gene is expressed as fold over control. Mean+SEM; n=12 to 14 (for **B**), n=6 (for **C**), n=8 (for **D**), n=5 (for **E** and **F**), *P<0.05; **P<0.01; ***P<0.001; ****P<0.0001, unpaired 2-tailed t tests. The numbers above bar graphs represent Δ Ct values (*Dnm3os*-reference gene). **G-I**, RT-qPCR analysis of indicated RNAs from total, nuclear, and cytoplasmic (Cyto) fractions. *U6* and *Neat1* RNA were used as positive controls for nuclear RNAs. Gene expression normalized to *Ppia* is expressed as fold over total. Mean+SEM; n=3. *P<0.05; **P<0.01; ****P<0.0001, unpaired 2-tailed t tests. **J, K**, Relative abundance of indicated RNAs in chromatin (Chr) and soluble nuclear extracts (SNE) after normalization with *Ppia* transcript (L). Mean+SEM; n=3. **P<0.01, unpaired 2-tailed t tests. **M, N**, RNA fluorescence in situ hybridization (RNA-FISH) analysis of *Dnm3os* (green spots) in macrophages. **M**, Control and palmitic acid (PA; 200 μ mol/L) treated RAW macrophages; **(N)** db/+ and db/db macrophages. Blue color nuclear staining with DAPI. Scale bars: 10 μ m (**M**) and 7 μ m (**N**).

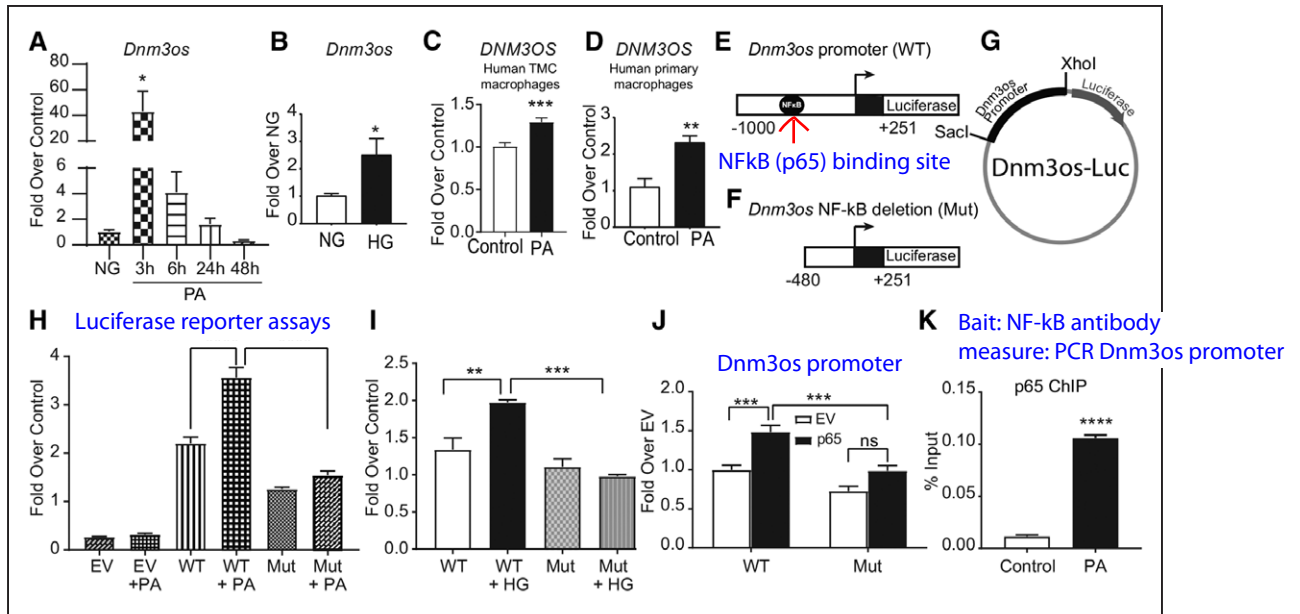


Figure 2. *Dnm3os* (dynamidin 3 opposite strand) is regulated by NF-κB under diabetic conditions. **A–D**, Palmitic acid (PA) and high glucose (HG) induce *Dnm3os* expression in macrophages. Real-time quantitative PCR (RT-qPCR) analysis of *Dnm3os* expression in bone marrow-derived macrophages (BMDMs) treated with PA (200 μmol/L) for indicated time points (**A**); with normal glucose (NG; 5.5 mmol/L) or HG (25 mmol/L) for 24 h (**B**). **C**, **D**, PA-induced *DNM3OS* expression in THP1 macrophages (TMC) and human primary macrophages. Mean±SEM; n=6 (for **A–D**), **P*<0.05, ***P*<0.01, ****P*<0.001, unpaired 2-tailed *t* tests. **E–G**, Schematic of the *Dnm3os* wild-type (WT) and NF-κB deletion mutant (Mut) promoters, and luciferase reporter plasmid with *Dnm3os* promoters. **H**, **I**, PA and HG activate *Dnm3os* promoter via NF-κB. Activity of *Dnm3os* WT and Mut promoters in RAW macrophages cotransfected with indicated reporter plasmids and control Renilla luciferase (REN) plasmid after treatment±PA (**H**) and HG or NG (**I**) for 24 h. Firefly luciferase activity normalized with REN expressed as fold over control cells. Empty vector (EV)-empty luciferase vector pGL4. Mean±SEM; n=6 (for **H**), n=3 (for **I**), ***P*<0.01; ****P*<0.001; *****P*<0.0001, using 1-way ANOVA, Tukey multiple comparison test. **J**, NF-κB (p65) transactivates *Dnm3os* promoter. Relative luciferase activity in RAW macrophages cotransfected with indicated reporter plasmids along with NF-κB expression vector (p65) or EV and internal control REN plasmid. Mean±SEM; n=5, ****P*<0.001, using 1-way ANOVA, Tukey multiple comparison test. **K**, Chromatin immunoprecipitation (ChIP) assays showing p65 enrichment at NF-κB binding site in *Dnm3os* promoter in macrophages treated±PA (200 μmol/L). Mean±SEM; n=3, *****P*<0.0001 using unpaired 2-tailed *t* tests.

+ 251 bp) and a mutant promoter (−480 to +251 bp) lacking the NF-κB site, upstream of firefly luciferase reporter gene (Figure 2E through 2G). Transient transfection of these constructs into RAW macrophages and luciferase assays showed that PA and HG increased the transcriptional activity of *Dnm3os* wild-type promoter, which was abrogated in NF-κB deletion mutant (Figure 2H and 2I). In addition, cotransfection with p65 (NF-κB active subunit) expression vector transactivated *Dnm3os* wild-type but not a mutant promoter in RAW macrophages (Figure 2J). Furthermore, ChIP assays with p65 antibody showed that PA treatment significantly increased p65 enrichment at the *Dnm3os* promoter compared with control in RAW macrophages (Figure 2K). These data clearly demonstrate that *Dnm3os* is upregulated by NF-κB binding to its promoter under diabetic conditions.

***Dnm3os* Overexpression Promotes Proinflammatory Functions in Macrophages**

Next, we examined the effect of *Dnm3os* overexpression in macrophages, mimicking its upregulation in diabetes mellitus. We cloned full-length *Dnm3os* into pcDNA3.1 expression vector (Figure II in the [online-only Data Supplement](#)) and generated RAW cell lines stably transfected with *Dnm3os* expression vector (RAW-*Dnm3os*) and empty pcDNA3.1 vector (RAW-EV). We then performed RNA-seq analysis in biological replicates using RNA extracted from these 2 cell lines (Figure III in the [online-only Data Supplement](#)). Correlation and principal component analysis showed good

correlation between the replicates (Figure IVA and IVB in the [online-only Data Supplement](#)). Two hundred three genes were upregulated and 113 downregulated in *Dnm3os* overexpressing macrophages (RAW-*Dnm3os*) versus control RAW-EV (FDR <0.1, log₂ fold change ≥0.5; Figure 3A; Figure IVC in the [online-only Data Supplement](#)). DAVID analysis of *Dnm3os*-induced genes showed enrichment of key macrophage phenotypes including phagocytosis, inflammation, immune response, cell activation, chemotaxis, and response to wounding (Figure 3B). Furthermore, gene set enrichment analysis³⁷ showed enrichment of gene sets related to macrophage activation in genes upregulated by *Dnm3os* overexpression (Figure 3C). Using RT-qPCR we validated several key inflammatory genes upregulated by *Dnm3os* overexpression in RAW-*Dnm3os* versus RAW-EV (Figure 3D through 3N), although few upregulated genes tested could not be validated (Figure V in the [online-only Data Supplement](#)). Interestingly, *Dnm3os* overexpression increased the expression of genes not only on chr1 on which it is located but also altered those present on other chromosomes (Figure 3O) suggesting both *cis*- and *trans*-actions. Furthermore, TF motif analysis showed enrichment of PU.1, NKx3-2, AP1, STAT, IRF1, REL binding sites in the promoters of upregulated genes (Figure 3P through 3U), whereas EBF1, REST, and KLF4 sites were enriched in downregulated genes (Figure 3V through 3X). In addition, immunoblotting of cell lysates showed that *Dnm3os* overexpression increased global levels of permissive histone modifications such as H3K9ac and H3K27ac compared with

RNA-seq
stable clone: RAW-Dnm3os

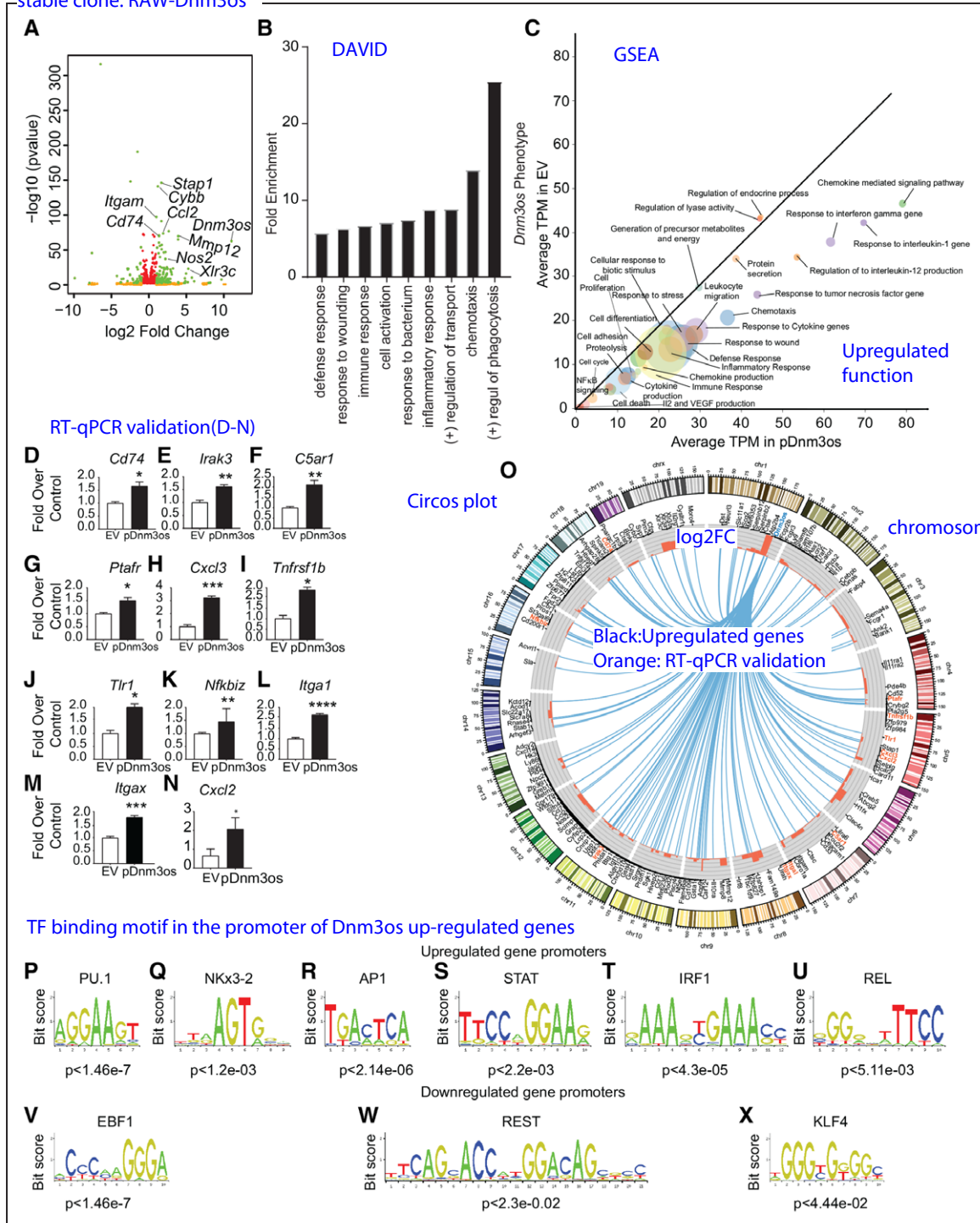


Figure 3. *Dnm3os* (dynamitin 3 opposite strand) overexpression promotes proinflammatory functions in macrophages. **A**, Volcano plot showing significantly upregulated and downregulated genes from RNA-seq data in *Dnm3os* stably overexpressing macrophage cell line RAW-Dnm3os (pDnm3os) vs control vector (RAW-empty vector [EV]). Genes depicted in green are those with $P_{adj} < 0.05$ and $\log_2FC > 0.6$; Orange: $P_{adj} > 0.05$ and $\log_2FC > 0.6$; and red: $P_{adj} < 0.05$ and $\log_2FC < -0.6$. **B**, DAVID analysis of *Dnm3os*-induced genes shows enrichment of key macrophage functions. **C**, Gene set enrichment analysis (GSEA) analysis of genes upregulated in RAW-Dnm3os macrophages. Significant biological process gene sets (empirical $P < 0.05$) below the diagonal line are upregulated. The size of the circle is proportional to the number of significantly altered genes ($0.5 < \log_2FC < -0.5$) within each pathway. **D-N**, Real-time quantitative PCR (RT-qPCR) validation of indicated *Dnm3os*-induced genes identified by RNA-seq in RAW-Dnm3os macrophages relative to RAW-EV. Mean \pm SEM; $n=3$, * $P < 0.05$; ** $P < 0.01$; *** $P < 0.001$; **** $P < 0.0001$ using unpaired 2-tailed t tests. **O**, Circos plot depicting the genes upregulated by *Dnm3os* overexpression in RAW-Dnm3os macrophages. Upregulated genes (black and orange color fonts) are connected to the *Dnm3os* locus on chr1 (blue font) by blue lines. Orange fonts indicate upregulated genes validated by RT-qPCR in panels. Outer circle represents chromosome ideograms (chr Y is not shown). Inner circle shows histograms (red color) representing \log_2FC of each gene. **P-X**, Motif analysis of upregulated (P-U) and downregulated (V-X) gene promoters in RAW-Dnm3os macrophages.

RAW-EV (Figure VI in the online-only Data Supplement). Together, these data suggest that overexpression of *Dnm3os* augments proinflammatory genes possibly via changes in epigenetic histone modifications in macrophages.

Dnm3os Enhances Inflammation and Phagocytosis

To further examine the function of *Dnm3os* and its target genes under diabetic conditions in vitro, we treated RAW-Dnm3os and RAW-EV macrophages with or without PA. *Dnm3os* was significantly increased by PA in both cell lines (Figure 4A)

along with several inflammatory genes (Figure 4B through 4E). Furthermore, PA-induced expression of *Il6*, *Tnf*, *Nos2*, and *Cd36* was significantly greater in RAW-Dnm3os macrophages (pDnm3os) relative to RAW-EV (Figure 4B through 4E), demonstrating that *Dnm3os* can further augment the proinflammatory effects of PA. Because lncRNAs can regulate nearby genes (*cis*- effects), we also tested if *Dnm3os* overexpression affects its nearby genes *Mettl13* and *Vamp4*. However, both these genes were not affected (Figure VII in the online-only Data Supplement).

anti-sense oligo

siRNA \rightarrow Dnm3os \rightarrow phagocytosis

1-way ANOVA, Tukey multiple comparison test

C: control
PA: palmitic acid

E. coli bioparticles (green)
phagocytosis

Downloaded from http://ahajournals.org by on June 16, 2019

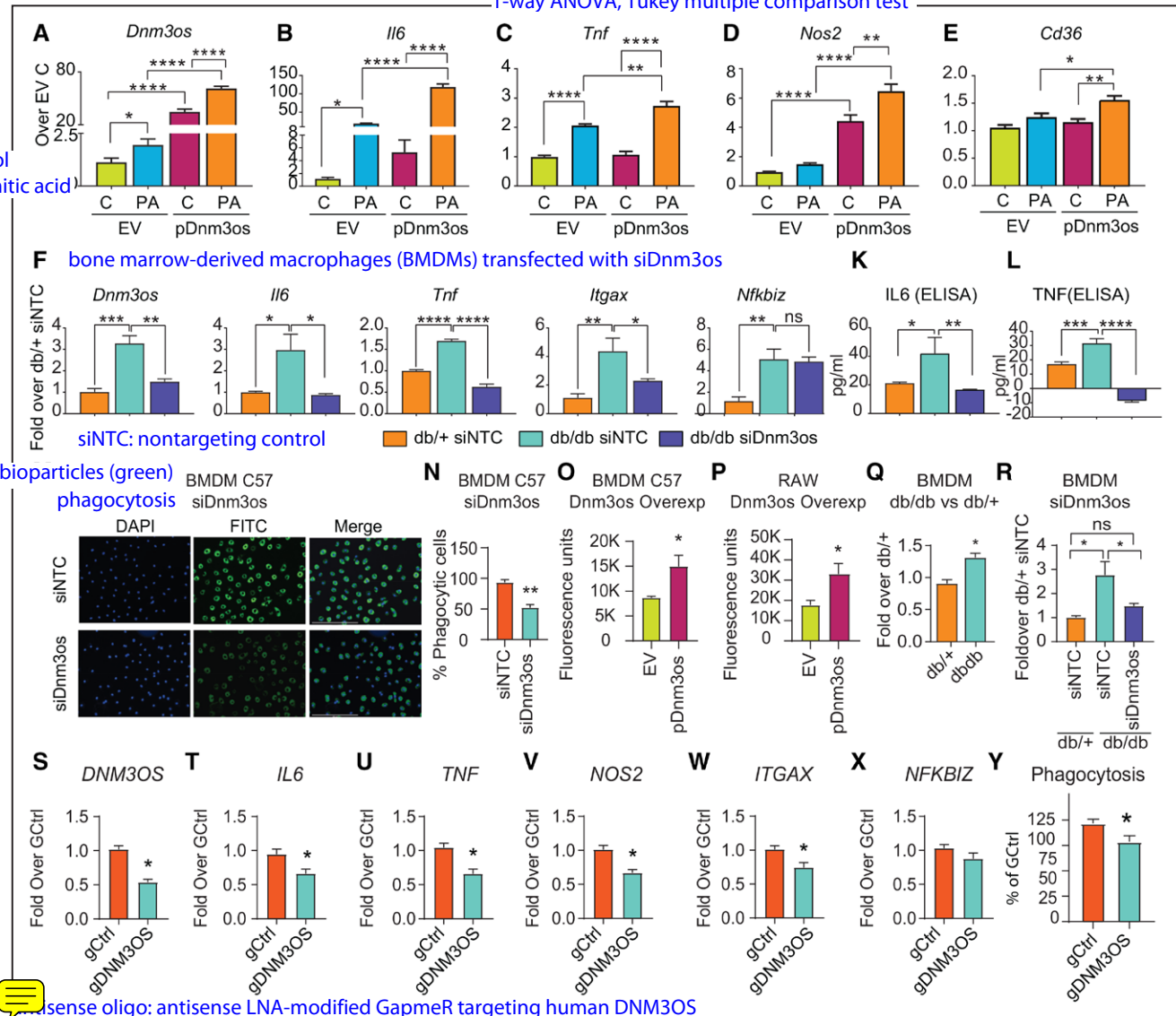
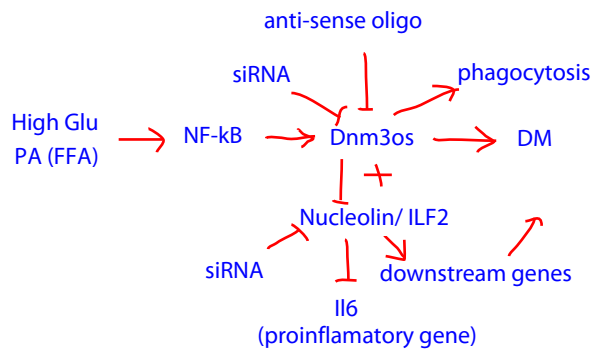
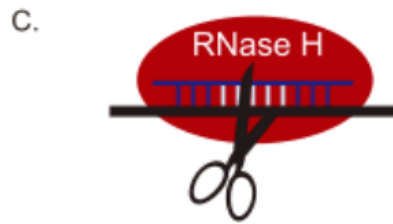
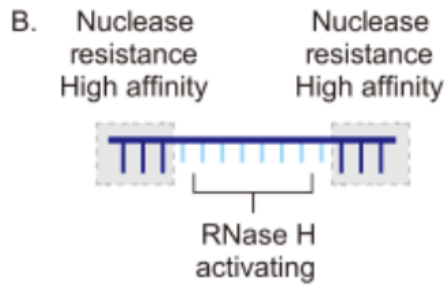


Figure 4. *Dnm3os* (dynamitin 3 opposite strand) promotes inflammation and phagocytosis. **A–E**, Bar graphs represent the expression of indicated genes in RAW-empty vector (EV) and RAW-Dnm3os (pDnm3os) macrophages without (C) and with palmitic acid (PA) treatment (24 h). Results are expressed as fold over untreated RAW-EV (EV, C). Mean+SEM; n=5 to 6, **P*<0.05; ***P*<0.01; *****P*<0.0001, 1-way ANOVA, Tukey multiple comparison test. **F–L**, Gene expression (real-time quantitative PCR [RT-qPCR]) and protein levels (ELISA) in bone marrow-derived macrophages (BMDMs) transfected with siDnm3os vs nontargeting control (siNTC) in db/db vs db/+ mice. Mean+SEM; n=4 to 6, **P*<0.05; ***P*<0.01; *****P*<0.0001, 1-way ANOVA, Tukey multiple comparison test. **M, N**, Effect of *Dnm3os* knockdown on phagocytosis. Representative images showing phagocytosis of FITC-labeled fluorescent *E. coli* bioparticles (green) in BMDMs (C57BL/6 mice) transfected with siDnm3os or control siNTC oligonucleotides (**M**) and quantification of phagocytosis (**N**). Mean+SEM; n=3, ***P*<0.01, unpaired 2-tailed *t* tests. Blue color-DAPI. **O, P**, Effect of *Dnm3os* overexpression on phagocytosis in C57BL/6 BMDMs (**O**); transiently transfected with *Dnm3os* vector (pDnm3os) vs pcDNA3.1 (EV), and RAW-Dnm3os (pDnm3os) vs RAW-EV (EV) macrophages (**P**). Phagocytosis assays were performed in 96 wells and fluorescence of internalized particles measured on a plate reader. Mean+SEM; **P*<0.05; n=4, unpaired 2-tailed *t* tests. **Q, R**, Phagocytosis assays were performed in BMDMs from db/+ and db/db mice without transfection (**Q**) or after transfection with siNTC (in db/+ and db/db) or siDnm3os (db/db) BMDMs (**R**) mean+SEM; **P*<0.05; n=5 to 6. **S–X**, Gene expression (**S–X**) and phagocytosis (**Y**) in THP1 macrophages after *DNM3OS* knockdown using GapmeR (gDNM3OS) vs control GapmeR (gCtrl). Mean+SEM, **P*<0.05, unpaired *t* test (n=6–9 for **S–X** and 9–10 for **Y**).



Small Activating RNAs (saRNAs): dsRNA which targets gene promoters to induce transcriptional gene activation in a process known as RNA activation (RNAa)



Next, we examined if *Dnm3os* knockdown can inhibit candidate genes that were found to be upregulated in *Dnm3os* overexpressing cells. *Dnm3os* knockdown was confirmed in RAW macrophages transfected with *Dnm3os* siRNA (siDnm3os) relative to nontargeting control siNTC (Figure VIIIA in the [online-only Data Supplement](#)). Furthermore, *Dnm3os* knockdown also significantly downregulated key inflammatory genes *Il6* and *Itgax* (but not *NFkbiz*; Figure VIIIB through VIIID in the [online-only Data Supplement](#)) that were upregulated by *Dnm3os*. To examine direct relevance in diabetic macrophages, we next examined whether siRNA-mediated *Dnm3os* knockdown has similar effects in BMDMs from diabetic db/db mice, which exhibit enhanced expression of *Dnm3os* and proinflammatory genes in culture (ex vivo) relative to BMDMs from nondiabetic db/+ mice. We transfected db/db BMDMs with siNTC or siDnm3os and, as control, db/+BMDMs with siNTC oligonucleotides. siDnm3os significantly downregulated the increased expression of *Dnm3os* in BMDMs from db/db mice (Figure 4F) and, in parallel, also suppressed diabetes mellitus-induced enhanced inflammatory gene expression (Figure 4G through 4I) and cytokine secretion (Figure 4K and 4L) relative to siNTC transfected control db/+BMDMs. However, siDnm3os did not affect changes in *Nfkbiz* (Figure 4J) or the host gene *Dnm3* (Figure IXA in the [online-only Data Supplement](#)). We also verified that the siRNA can target nuclear *Dnm3os* because siDnm3os significantly downregulated *Dnm3os* expression in nuclear fractions from db/db BMDMs versus siNTC transfected cells, but not in the cytoplasmic fractions where *Dnm3os* expression is much lower (Figure IXB through IXC in the [online-only Data Supplement](#)). Together, these results support a role for *Dnm3os* in diabetes mellitus-induced enhanced inflammatory phenotype of macrophages.

We next examined whether *Dnm3os* regulates phagocytosis, an important function of macrophages, by incubating fluorescently labeled *E. coli* bioparticles with macrophages after *Dnm3os* knockdown or overexpression. siDnm3os significantly inhibited phagocytosis compared with siNTC in BMDMs from control C57BL/6 mice (Figure 4M and 4N). In contrast, *Dnm3os* overexpression in BMDMs (via transient transfection), and RAW-Dnm3os macrophages significantly increased phagocytosis relative to EV (Figure 4O and 4P). Moreover, BMDMs from db/db mice exhibited increased phagocytosis relative to db/+ (Figure 4Q) that was attenuated by siDnm3os (Figure 4R). Interestingly, GapmeR-mediated human *DNM3OS* knockdown also significantly reduced inflammatory genes and phagocytosis in THP1 macrophages, suggesting similar mechanisms in human cells (Figure 4S through 4Y). These results demonstrate that *Dnm3os* promotes inflammation and phagocytosis in macrophages.

***Dnm3os* Interacts With Nuclear Proteins in Macrophages**

Interaction with key nuclear proteins is a major mechanism by which lncRNAs regulate gene expression.¹¹ Therefore, to gain additional insights into the mechanisms of *Dnm3os* actions, RNA pull-down assays⁴³ were performed to identify interacting protein partners of *Dnm3os*. *Dnm3os* sense and antisense (negative control) transcripts were biotinylated by in

vitro transcription and RNA integrity as well as biotinylation efficiency of probes verified by denaturing gel electrophoresis and dot blot assays, respectively (Figure X in the [online-only Data Supplement](#)). Nuclear extracts from normal mouse PMs were incubated with these 2 biotinylated probes and RNA-protein complexes resolved on an SDS-PAGE gel (Figure 5A). Parallel protein bands in different regions of the gel from sense and antisense lanes were subjected to mass spectrometry analysis. Results showed that several nuclear proteins were specifically associated with *Dnm3os*-sense strand, but not with antisense (Figure 5B). These included nucleolin, ILF-2, actin-related protein 3, RNA-binding protein Ralv short isoform, heterogeneous nuclear ribonucleoproteins U like protein 2, and heterogeneous ribonucleoprotein A1 isoform. To validate these interactions, RNA-protein complexes from RNA-pull down assays were immunoblotted with antibodies to nucleolin and ILF-2. Results showed that both proteins interacted specifically with sense *Dnm3os* RNA but not antisense RNA (Figure 5C and 5D). Furthermore, RNA fluorescence in situ hybridization with *Dnm3os* probe coupled with immunofluorescence using specific antibodies also showed the nuclear colocalization of *Dnm3os* with nucleolin and ILF-2 in both control and PA-treated macrophages (Figure 5E and 5F). These results clearly demonstrate that *Dnm3os* interacts with nucleolin and ILF-2 in macrophages.

Nucleolin Modulates Proinflammatory and Epigenetic Actions of *Dnm3os* in Macrophages

Nucleolin is a multifunctional nucleolar protein⁴⁴ and one of its key functions includes regulation of chromatin structure. But its function in macrophages in diabetes mellitus is unknown. Recent studies suggested an atheroprotective function in macrophages⁴⁵ and anti-inflammatory effects in HeLa cells.⁴⁶ Therefore, we hypothesized that nucleolin may negatively regulate proinflammatory functions of *Dnm3os* and that inhibition of such interactions under diabetic conditions may promote inflammatory gene regulation. To test this, we checked nucleolin protein levels under diabetic conditions. PA and HG plus PA treatment significantly decreased nucleolin protein levels in RAW macrophages compared with the normal glucose-treated cells (Figure 6A and 6B). We also found that nucleolin protein levels were significantly reduced in BMDMs from diabetic db/db mice relative to control db/+ (Figure 6C and 6D). This supports the notion that inhibition of nucleolin under diabetic conditions in vivo might promote inflammatory gene expression.

Next, we examined the effect of nucleolin knockdown on inflammatory gene expression in *Dnm3os* overexpressing macrophages. Transfection with nucleolin siRNA (siNcl) significantly inhibited nucleolin mRNA and protein versus siNTC in both RAW-Dnm3os and RAW-EV macrophages (Figure 6E through 6G). Furthermore, nucleolin knockdown increased the expression of proinflammatory gene *Il6* in RAW-EV macrophages and this effect was further significantly enhanced in RAW-Dnm3os macrophages (Figure 6H).

Next, we tested whether *Dnm3os* has *trans*-effects on inflammatory genes by augmenting permissive chromatin modifications like H3K9ac at their promoters. We examined the role of such epigenetic mechanisms in *Il6* regulation

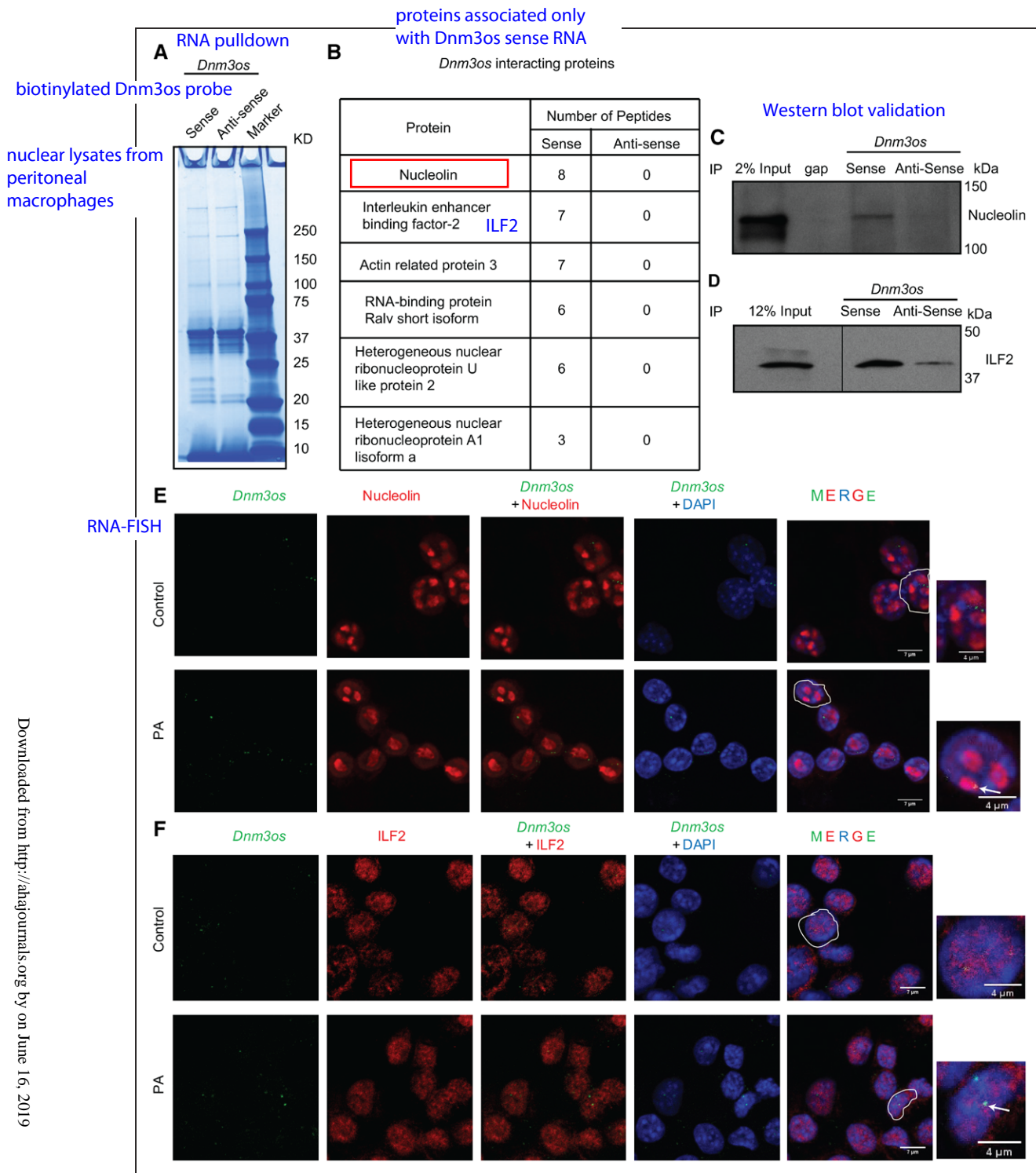


Figure 5. *Dnm3os* (dynamin 3 opposite strand) interacts with key nuclear proteins in macrophages. **A**, Gel image showing Simply Blue safe staining of proteins associated with biotinylated *Dnm3os* sense and control antisense RNAs using nuclear lysates from peritoneal macrophages (PMs). Proteins from both lanes were analyzed by mass spectrometry. **B**, List of top proteins associated only with *Dnm3os* sense RNA. **C**, **D**, Images of RNA pull-down followed by Western blotting with nucleolin and ILF-2 (interleukin enhancer-binding factor 2) antibodies. **E–F**, RNA fluorescence in situ hybridization (RNA-FISH) coupled with immunofluorescence using *Dnm3os* probe (green color) and nucleolin or ILF-2 antibodies (red color) in control and palmitic acid (PA) treated RAW coupled macrophages. Scale bar 7 μ m in all panels, except in enlarged images scale bars which are 4 μ m. Arrows indicate location of *Dnm3os*.

by *Dnm3os*-nucleolin interactions using ChIP assays with H3K9ac antibody and qPCR with primers specific to *Il6* promoter (Figure 6I). Interestingly, nucleolin depletion (siNcl) increased the enrichment of H3K9ac at *Il6* promoter in control RAW-EV macrophages relative to siNTC (Figure 6J).

Moreover, *Dnm3os* overexpression also increased H3K9ac at the *Il6* promoter in RAW-*Dnm3os* macrophages and notably, this effect was further enhanced by nucleolin depletion (Figure 6J). However, nucleolin knockdown did not alter H3K9ac at *Tnf* and *Nos2* promoters (Figure XI in the

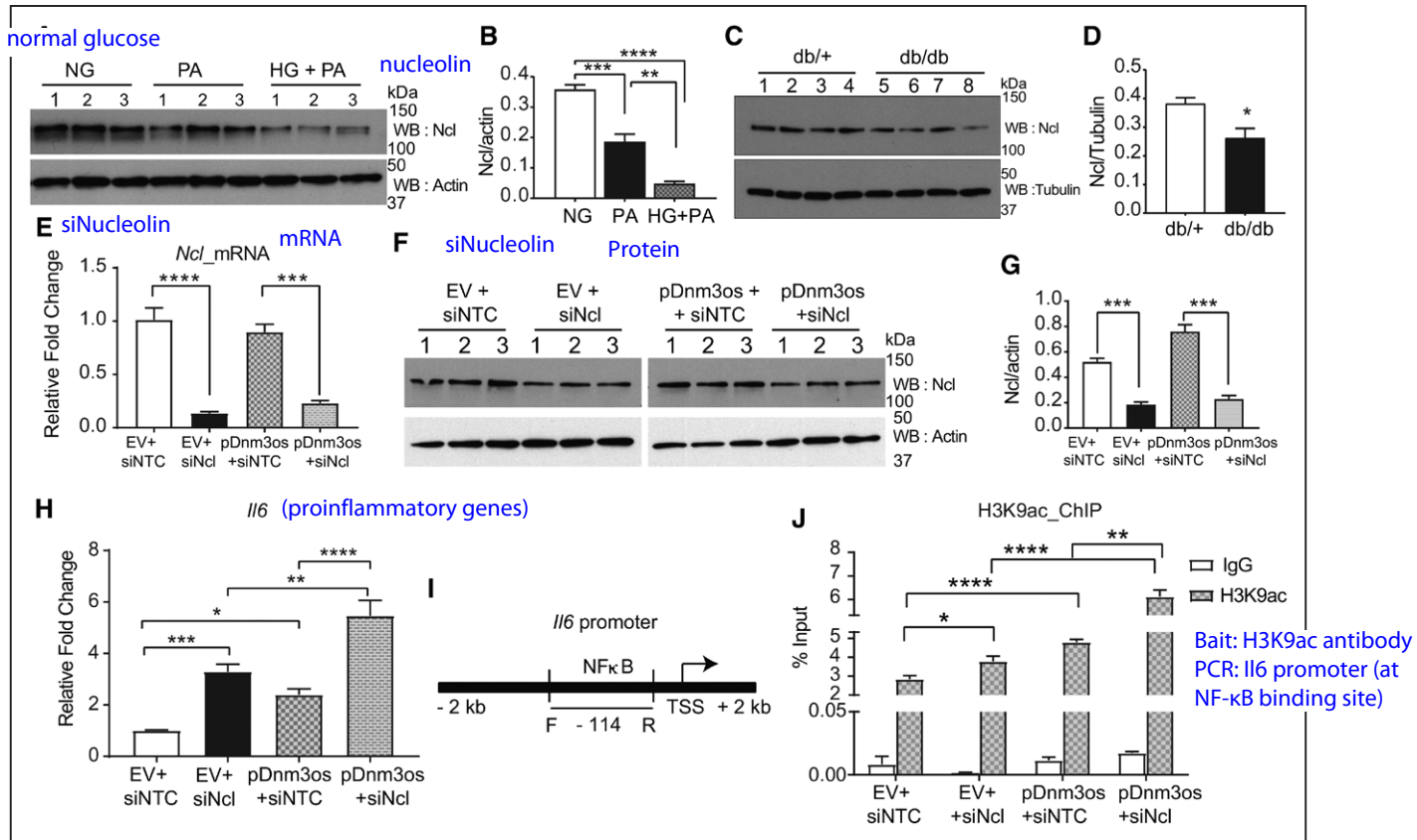


Figure 6. Nucleolin modulates proinflammatory and epigenetic actions of *Dnm3os* (dynamins 3 opposite strand) in macrophages. **A, B,** Immunoblots showing nucleolin protein levels in macrophages after treatment with palmitic acid (PA; for 24 h) and high glucose (HG)+PA (72 h for HG and 24 h for PA) compared with normal glucose (NG). **B,** Quantification of nucleolin protein in Western blots. Mean+SEM; n=3, ** P <0.01, *** P <0.001, **** P <0.0001, 1-way ANOVA, Tukey multiple comparison test. **C, D,** Nucleolin protein levels and its quantification in bone marrow-derived macrophages (BMDMs) from db/db vs db/+ mice. Mean+SEM; n=4, * P <0.05, using unpaired 2-tailed t tests. **E–G,** Downregulation of nucleolin mRNA (**E**) and protein (**F, G**) levels using nucleolin siRNA (siNcl) vs siNTC in RAW-EV (empty vector [EV]) and RAW-Dnm3os (pDnm3os) macrophages. Mean+SEM; n=3, *** P <0.001, **** P <0.0001, unpaired 2-tailed t tests (for **E** and **G**). **H,** Bar graph showing *Il6* expression in EV and RAW-Dnm3os macrophages after transfection with siNTC and siNcl. **I,** Schematic of *Il6* promoter showing NF- κ B binding sites and location of PCR primers. **J,** Bar graphs represent H3K9ac enrichment on the *Il6* promoter (at NF- κ B binding site) in RAW-EV and RAW-Dnm3os macrophages transfected with siNTC or siNcl. Data are shown as percent input. Mean+SEM; n=6 (for **H**) and 5 to 6 (for **J**), * P <0.05, ** P <0.01; *** P <0.001; **** P <0.0001, 1-way ANOVA, Tukey multiple comparison tests (for **H** and **J**).

online-only Data Supplement). It is possible that other active chromatin marks beside H3K9ac may be involved in *Dnm3os*-mediated increases in other target inflammatory genes besides *Il6*. Thus, *Dnm3os*-nucleolin interactions can regulate, in part, the macrophage inflammatory phenotype via epigenetic mechanisms such as increased permissive histone modifications and chromatin relaxation.

Discussion

In this study, we demonstrate a novel mechanism of enhanced macrophage inflammatory phenotype in diabetes mellitus by lncRNA *Dnm3os*. Macrophages are key players in promoting inflammation implicated in insulin resistance, lipid accumulation in the vessel wall, and related vascular complications. Furthermore, increased oxidative stress in diabetes mellitus increases formation of oxidized LDL (low-density lipoprotein), which further enhances inflammation. Concerted actions of all these events play important roles in the initiation and progression of atherosclerosis.³ Multiple signaling and epigenetic mechanisms have been implicated in augmenting these processes under diabetic states. Notably, lncRNAs have been recently discovered to play a role in

macrophage inflammation under normal and diabetic conditions.^{20,24} Here, we showed that the expression of lncRNA *Dnm3os* is increased in macrophages derived from several mouse models of metabolic disorders including type 1 diabetic, T2D, obesity, and insulin resistance. *Dnm3os* expression was upregulated in BMDMs from both male (Figure 1) and female db/db mice (Figure XII in the online-only Data Supplement). Moreover, *Dnm3os* is also upregulated in STZ-injected Apoe^{-/-} mice, a model of diabetes mellitus-induced accelerated atherosclerosis⁴¹ indicating its association with diabetic vascular diseases. We confirmed that *Dnm3os* lacks coding potential using PhyloCSF, CPAT, and macrophage ribosome profiling databases, and in vitro transcription/translation assays (Figure XIII A through XIII C in the online-only Data Supplement). Moreover, *Dnm3os* is conserved in humans and expressed in multiple tissues including adipose, aorta, and whole blood (Figure XIV in the online-only Data Supplement). Interestingly, we found that *Dnm3os* is also upregulated in monocytes from T2D patients. These in vivo findings suggest that *Dnm3os* is regulated by hyperglycemia and hyperlipidemia in diabetes mellitus. Accordingly, our in vitro experiments clearly demonstrated that HG as well as

PA, a free fatty acid abundant in obesity and T2D, increased *Dnm3os* expression in macrophages.

Reports show that *Dnm3os* is regulated by Twist and PPAR- α (peroxisome proliferator-activated receptor- α) in cardiac and endothelial cells.^{47,48} Our studies show that HG and PA activate the *Dnm3os* promoter via NF- κ B. PA can increase inflammatory gene expression via TLR4 (Toll-like receptor 4) activation, and HG can via activation of tyrosine kinases and protein kinase C. Both stimuli also activate NF- κ B TF to induce inflammatory genes. Our results using macrophages derived from diabetic db/db mice support a role for *Dnm3os* in mediating diabetes mellitus-induced proinflammatory phenotype. Previous studies showed activation of NF- κ B in this ex vivo model of diabetes mellitus-induced accelerated inflammation and macrophage activation.⁴ Thus, activation of NF- κ B by several factors in obesity and diabetes mellitus can increase *Dnm3os* in macrophages to further augment macrophage dysfunction. However, NF- κ B activation in diabetes mellitus can clearly have effects on multiple inflammatory pathways and, whether *Dnm3os* mediates some or many of these effects in vivo has to be determined.

Mechanistically, lncRNAs regulate gene expression via distinct processes that promote or inhibit recruitment of transcription and epigenetic regulators to modulate chromatin structure.¹⁵ In macrophages, lncRNAs *THRIL*, *EPS*, and lncRNA-COX-2 interact with RNA-binding proteins of hnRNP family to regulate NF- κ B function and dysregulate chromatin structure around inflammatory genes.²⁰ We found that *Dnm3os* is highly enriched in the nucleus and associated with chromatin, supporting its role in gene regulation. We also observed *Dnm3os* interacts with nucleolin, ILF-2, and several RNA-binding proteins including hnRNPs. Interaction of hnRNPs with lncRNAs has been widely demonstrated in macrophages.²⁰ ILF-2 regulates *IL2* expression in T-cells, but its function in other cell types is unclear.⁴⁹ Nucleolin, a 77 kDa protein highly enriched in the nucleolus, has multiple functions especially in chromatin structure and transcription.⁴⁴ However, nucleolin function in diabetes mellitus and lncRNA-mediated gene regulation has not been previously examined. Our new results demonstrate that *Dnm3os*-nucleolin interaction could be a key mechanism regulating inflammatory phenotype of macrophages. We found that nucleolin inhibited *Il6* gene expression which suggests anti-inflammatory functions. Moreover, *Dnm3os*-induced *Il6* gene expression was further enhanced after nucleolin knockdown in macrophages. In support of our data, studies in HeLa cells showed nucleolin downregulation increased *IL6* expression,⁴⁶ whereas in macrophages, nucleolin overexpression inhibited oxidized-LDL-induced foam cell formation through enhancing ABCA1 (ATP-binding cassette sub family A member 1) expression.⁴⁵ Further investigation is needed to determine whether *Dnm3os* can modulate macrophage foam cell formation through interactions with nucleolin. Our studies suggest that nucleolin-*Dnm3os* interaction inhibits inflammatory genes possibly via promoting repressive chromatin structure. Because diabetic conditions increase *Dnm3os* and decrease nucleolin levels, consequently, this can promote permissive histone modifications such as H3K9ac and open chromatin formation at inflammatory genes. Nucleolin functions are

regulated by multiple posttranslational modifications including phosphorylation and acetylation, which could affect its protein stability.^{44,50} Further studies are needed to examine how such complex regulatory mechanisms are involved in the downregulation of nucleolin by HG and PA.

We also observed *Dnm3os* increases phagocytosis in macrophages. It is possible *Dnm3os* enhances phagocytosis via upregulation of *Cd36* (Figure 4E), a key regulator of phagocytosis and foam cell formation.⁵¹ The role of phagocytosis in atherosclerosis is quite complex. Increased phagocytosis promotes excess uptake of oxidized lipids and foam cell formation, key steps in the initiation of lesions. Furthermore, in advanced complex lesions, nonspecific increases in phagocytosis of apoptotic cells could affect plaque stability.⁵² Thus, macrophage *Dnm3os* upregulation in diabetes mellitus may affect initiation and progression of vascular disease. However, further in vivo studies are needed to determine whether *Dnm3os* also plays a role in clearance of pathogens and apoptotic cells, important events in infection and atherosclerosis, respectively.

Previous studies in cardiac and endothelial cells showed a role for *Dnm3os* during heart failure and hypertension,^{47,48} but they examined its function as a host gene for miR-199 and miR-214, and not as a lncRNA. In our study, overexpression of miR-199a and miR-214 did not affect most of the tested *Dnm3os* target genes (Figure XV in the [online-only Data Supplement](#)), suggesting mostly miRNA-independent effects for *Dnm3os* in diabetic macrophages. Other studies have also shown similar lncRNA functions of miRNA host genes in different cell types.^{24,53}

Taken together, our results demonstrate lncRNA *Dnm3os*-mediated novel mechanisms for increased macrophage inflammatory gene expression in diabetes mellitus. Under normal conditions, nucleolin interacts with and prevents the functional ability of *Dnm3os* to increase enrichment of permissive histone modifications like H3K9ac at promoters of inflammatory genes such as *Il6*. But, under diabetic conditions, increased *Dnm3os* and reduced nucleolin levels disrupt such interactions, allowing *Dnm3os* to enhance promoter H3K9ac, likely via recruitment of histone acetyltransferases, thereby leading to chromatin relaxation, upregulation of target inflammatory, and macrophage dysfunction (Figure XVI in the [online-only Data Supplement](#)). As certain human macrophage lncRNAs have also recently been associated with cardiometabolic disorders,⁵⁴ increased understanding of macrophage lncRNAs and their interacting proteins could aid the development of better therapies for inflammatory diabetic complications.

Sources of Funding

This study was supported by grants from the National Institutes of Health (NIH), R01 DK065073, R01 HL106089, and R01 DK081705 (to R. Natarajan). Research reported in this publication included work performed in the following Campus Cores: Integrative Genomics, DNA/RNA synthesis, and Mass Spectrometry and Proteomics (supported by the National Cancer Institute of the NIH under award number P30CA33572), and The Light Microscopy Core.

Disclosures

None.

References

- Beckman JA, Creager MA, Libby P. Diabetes and atherosclerosis: epidemiology, pathophysiology, and management. *JAMA*. 2002;287:2570–2581.
- Olefsky JM, Glass CK. Macrophages, inflammation, and insulin resistance. *Annu Rev Physiol*. 2010;72:219–246. doi: 10.1146/annurev-physiol-021909-135846.
- Bornfeldt KE, Tabas I. Insulin resistance, hyperglycemia, and atherosclerosis. *Cell Metab*. 2011;14:575–585. doi: 10.1016/j.cmet.2011.07.015.
- Li SL, Reddy MA, Cai Q, Meng L, Yuan H, Lanting L, Natarajan R. Enhanced proatherogenic responses in macrophages and vascular smooth muscle cells derived from diabetic db/db mice. *Diabetes*. 2006;55:2611–2619. doi: 10.2337/db06-0164.
- Nagareddy PR, Murphy AJ, Storzaker RA, Hu Y, Yu S, Miller RG, Ramkhalawon B, Distel E, Westerterp M, Huang LS, Schmidt AM, Orchard TJ, Fisher EA, Tall AR, Goldberg IJ. Hyperglycemia promotes myelopoiesis and impairs the resolution of atherosclerosis. *Cell Metab*. 2013;17:695–708. doi: 10.1016/j.cmet.2013.04.001.
- Natarajan R, Nadler JL. Lipid inflammatory mediators in diabetic vascular disease. *Arterioscler Thromb Vasc Biol*. 2004;24:1542–1548. doi: 10.1161/01.ATV.0000133606.69732.4c.
- Yan SF, Ramasamy R, Schmidt AM. Mechanisms of disease: advanced glycation end-products and their receptor in inflammation and diabetes complications. *Nat Clin Pract Endocrinol Metab*. 2008;4:285–293. doi: 10.1038/ncpendmet0786.
- Brownlee M. Biochemistry and molecular cell biology of diabetic complications. *Nature*. 2001;414:813–820. doi: 10.1038/414813a.
- Rask-Madsen C, King GL. Vascular complications of diabetes: mechanisms of injury and protective factors. *Cell Metab*. 2013;17:20–33. doi: 10.1016/j.cmet.2012.11.012.
- Reddy MA, Zhang E, Natarajan R. Epigenetic mechanisms in diabetic complications and metabolic memory. *Diabetologia*. 2015;58:443–455. doi: 10.1007/s00125-014-3462-y.
- Mercer TR, Mattick JS. Structure and function of long noncoding RNAs in epigenetic regulation. *Nat Struct Mol Biol*. 2013;20:300–307. doi: 10.1038/nsmb.2480.
- Quinn JJ, Chang HY. Unique features of long non-coding RNA biogenesis and function. *Nat Rev Genet*. 2016;17:47–62. doi: 10.1038/nrg.2015.10.
- Li W, Notani D, Rosenfeld MG. Enhancers as non-coding RNA transcription units: recent insights and future perspectives. *Nat Rev Genet*. 2016;17:207–223. doi: 10.1038/nrg.2016.4.
- Kato M, Wang M, Chen Z, Bhatt K, Oh HJ, Lanting L, Deshpande S, Jia Y, Lai JY, O'Connor CL, Wu Y, Hodgin JB, Nelson RG, Bitzer M, Natarajan R. An endoplasmic reticulum stress-regulated lncRNA hosting a microRNA megacluster induces early features of diabetic nephropathy. *Nat Commun*. 2016;7:12864. doi: 10.1038/ncomms12864.
- Rinn JL, Chang HY. Genome regulation by long noncoding RNAs. *Annu Rev Biochem*. 2012;81:145–166. doi: 10.1146/annurev-biochem-051410-092902.
- Uchida S, Dimmeler S. Long noncoding RNAs in cardiovascular diseases. *Circ Res*. 2015;116:737–750. doi: 10.1161/CIRCRESAHA.116.302521.
- Long J, Badal SS, Ye Z, Wang Y, Ayanga BA, Galvan DL, Green NH, Chang BH, Overbeek PA, Danesh FR. Long noncoding RNA Tug1 regulates mitochondrial bioenergetics in diabetic nephropathy. *J Clin Invest*. 2016;126:4205–4218. doi: 10.1172/JCI87927.
- Yan B, Yao J, Liu JY, Li XM, Wang XQ, Li YJ, Tao ZF, Song YC, Chen Q, Jiang Q. lncRNA-MIAT regulates microvascular dysfunction by functioning as a competing endogenous RNA. *Circ Res*. 2015;116:1143–1156. doi: 10.1161/CIRCRESAHA.116.305510.
- Leung A, Natarajan R. Long noncoding RNAs in diabetes and diabetic complications [published online ahead of print October 30, 2017]. *Antioxid Redox Signal*. doi: 10.1089/ars.2017.7315.
- Chen YG, Satpathy AT, Chang HY. Gene regulation in the immune system by long noncoding RNAs. *Nat Immunol*. 2017;18:962–972. doi: 10.1038/ni.3771.
- Li Z, Chao TC, Chang KY, Lin N, Patil VS, Shimizu C, Head SR, Burns JC, Rana TM. The long noncoding RNA THRIL regulates TNF α expression through its interaction with hnRNPL. *Proc Natl Acad Sci USA*. 2014;111:1002–1007. doi: 10.1073/pnas.1313768111.
- Carpenter S, Aiello D, Atianand MK, Ricci EP, Gandhi P, Hall LL, Byron M, Monks B, Henry-Bezy M, Lawrence JB, O'Neill LA, Moore MJ, Caffrey DR, Fitzgerald KA. A long noncoding RNA mediates both activation and repression of immune response genes. *Science*. 2013;341:789–792. doi: 10.1126/science.1240925.
- Atianand MK, Hu W, Satpathy AT, et al. A long noncoding RNA lincRNA-EPS acts as a transcriptional brake to restrain inflammation. *Cell*. 2016;165:1672–1685. doi: 10.1016/j.cell.2016.05.075.
- Reddy MA, Chen Z, Park JT, Wang M, Lanting L, Zhang Q, Bhatt K, Leung A, Wu X, Putta S, Sætrom P, Devaraj S, Natarajan R. Regulation of inflammatory phenotype in macrophages by a diabetes-induced long noncoding RNA. *Diabetes*. 2014;63:4249–4261. doi: 10.2337/db14-0298.
- Jin W, Reddy MA, Chen Z, Putta S, Lanting L, Kato M, Park JT, Chandra M, Wang C, Tangirala RK, Natarajan R. Small RNA sequencing reveals microRNAs that modulate angiotensin II effects in vascular smooth muscle cells. *J Biol Chem*. 2012;287:15672–15683. doi: 10.1074/jbc.M111.322669.
- Werner MS, Ruthenburg AJ. Nuclear fractionation reveals thousands of chromatin-tethered noncoding RNAs adjacent to active genes. *Cell Rep*. 2015;12:1089–1098. doi: 10.1016/j.celrep.2015.07.033.
- Sahar S, Reddy MA, Wong C, Meng L, Wang M, Natarajan R. Cooperation of SRC-1 and p300 with NF-kappaB and CREB in angiotensin II-induced IL-6 expression in vascular smooth muscle cells. *Arterioscler Thromb Vasc Biol*. 2007;27:1528–1534. doi: 10.1161/ATVBAHA.107.145862.
- Das S, Senapati P, Chen Z, Reddy MA, Ganguly R, Lanting L, Mandi V, Bansal A, Leung A, Zhang S, Jia Y, Wu X, Schones DE, Natarajan R. Regulation of angiotensin II actions by enhancers and super-enhancers in vascular smooth muscle cells. *Nat Commun*. 2017;8:1467. doi: 10.1038/s41467-017-01629-7.
- Cong R, Das S, Ugrinova I, Kumar S, Mongelard F, Wong J, Bouvet P. Interaction of nucleolin with ribosomal RNA genes and its role in RNA polymerase I transcription. *Nucleic Acids Res*. 2012;40:9441–9454. doi: 10.1093/nar/gks720.
- Orlando DA, Chen MW, Brown VE, Solanki S, Choi YJ, Olson ER, Fritz CC, Bradner JE, Guenther MG. Quantitative ChIP-Seq normalization reveals global modulation of the epigenome. *Cell Rep*. 2014;9:1163–1170. doi: 10.1016/j.celrep.2014.10.018.
- de Planell-Saguer M, Rodicio MC, Mourelatos Z. Rapid in situ codetection of noncoding RNAs and proteins in cells and formalin-fixed paraffin-embedded tissue sections without protease treatment. *Nat Protoc*. 2010;5:1061–1073. doi: 10.1038/nprot.2010.62.
- Rinn JL, Kertesz M, Wang JK, Squazzo SL, Xu X, Bruggmann SA, Goodnough LH, Helms JA, Farnham PJ, Segal E, Chang HY. Functional demarcation of active and silent chromatin domains in human HOX loci by noncoding RNAs. *Cell*. 2007;129:1311–1323. doi: 10.1016/j.cell.2007.05.022.
- Trapnell C, Pachter L, Salzberg SL. TopHat: discovering splice junctions with RNA-Seq. *Bioinformatics*. 2009;25:1105–1111. doi: 10.1093/bioinformatics/btp120.
- Robinson MD, McCarthy DJ, Smyth GK. edgeR: a Bioconductor package for differential expression analysis of digital gene expression data. *Bioinformatics*. 2010;26:139–140. doi: 10.1093/bioinformatics/btp616.
- Love MI, Anders S, Kim V, Huber W. RNA-Seq workflow: gene-level exploratory analysis and differential expression. *F1000Res*. 2015;4:1070. doi: 10.12688/f1000research.7035.1.
- Huang da W, Sherman BT, Lempicki RA. Systematic and integrative analysis of large gene lists using DAVID bioinformatics resources. *Nat Protoc*. 2009;4:44–57. doi: 10.1038/nprot.2008.211.
- Subramanian A, Tamayo P, Mootha VK, Mukherjee S, Ebert BL, Gillette MA, Paulovich A, Pomeroy SL, Golub TR, Lander ES, Mesirov JP. Gene set enrichment analysis: a knowledge-based approach for interpreting genome-wide expression profiles. *Proc Natl Acad Sci USA*. 2005;102:15545–15550. doi: 10.1073/pnas.0506580102.
- Krzywinski M, Schein J, Birol I, Connors J, Gascoyne R, Horsman D, Jones SJ, Marra MA. Circos: an information aesthetic for comparative genomics. *Genome Res*. 2009;19:1639–1645. doi: 10.1101/gr.092759.109.
- Thomas-Chollier M, Hufton A, Heinig M, O'Keefe S, Masri NE, Roeder HG, Manke T, Vingron M. Transcription factor binding predictions using TRAP for the analysis of ChIP-seq data and regulatory SNPs. *Nat Protoc*. 2011;6:1860–1869. doi: 10.1038/nprot.2011.409.
- Wang P, Xu J, Wang Y, Cao X. An interferon-independent lncRNA promotes viral replication by modulating cellular metabolism. *Science*. 2017;358:1051–1055. doi: 10.1126/science.aao0409.
- Bucciarelli LG, Wendt T, Qu W, Lu Y, Lalla E, Rong LL, Goova MT, Moser B, Kislinger T, Lee DC, Kashyap Y, Stern DM, Schmidt AM. RAGE blockade stabilizes established atherosclerosis in diabetic apolipoprotein E-null mice. *Circulation*. 2002;106:2827–2835.
- Wasserman WW, Sandelin A. Applied bioinformatics for the identification of regulatory elements. *Nat Rev Genet*. 2004;5:276–287. doi: 10.1038/nrg1315.

43. Huarte M, Guttman M, Feldser D, Garber M, Koziol MJ, Kenzelmann-Broz D, Khalil AM, Zuk O, Amit I, Rabani M, Attardi LD, Regev A, Lander ES, Jacks T, Rinn JL. A large intergenic noncoding RNA induced by p53 mediates global gene repression in the p53 response. *Cell*. 2010;142:409–419. doi: 10.1016/j.cell.2010.06.040.
44. Cong R, Das S, Bouvet P. The multiple properties and functions of nucleolin. In: Olson M, ed. *The Nucleolus*. New York: Springer; 2011:185–212.
45. Li Y, Jiang B, Liang P, Tong Z, Liu M, Lv Q, Liu Y, Liu X, Tang Y, Xiao X. Nucleolin protects macrophages from oxLDL-induced foam cell formation through up-regulating ABCA1 expression. *Biochem Biophys Res Commun*. 2017;486:364–371. doi: 10.1016/j.bbrc.2017.03.047.
46. Kumar S, Gomez EC, Chalabi-Dchar M, Rong C, Das S, Ugrinova I, Gaume X, Monier K, Mongelard F, Bouvet P. Integrated analysis of mRNA and miRNA expression in HeLa cells expressing low levels of Nucleolin. *Sci Rep*. 2017;7:9017. doi: 10.1038/s41598-017-09353-4.
47. Li C, Mpollo MS, Gonsalves CS, Tahara SM, Malik P, Kalra VK. Peroxisome proliferator-activated receptor- α -mediated transcription of miR-199a2 attenuates endothelin-1 expression via hypoxia-inducible factor-1 α . *J Biol Chem*. 2014;289:36031–36047. doi: 10.1074/jbc.M114.600775.
48. el Azzouzi H, Leptidis S, Dirks E, et al. The hypoxia-inducible microRNA cluster miR-199a~214 targets myocardial PPAR δ and impairs mitochondrial fatty acid oxidation. *Cell Metab*. 2013;18:341–354. doi: 10.1016/j.cmet.2013.08.009.
49. Zhao G, Shi L, Qiu D, Hu H, Kao PN. NF45/ILF2 tissue expression, promoter analysis, and interleukin-2 transactivating function. *Exp Cell Res*. 2005;305:312–323. doi: 10.1016/j.yexcr.2004.12.030.
50. Das S, Cong R, Shandilya J, Senapati P, Moindrot B, Monier K, Delage H, Mongelard F, Kumar S, Kundu TK, Bouvet P. Characterization of nucleolin K88 acetylation defines a new pool of nucleolin colocalizing with pre-mRNA splicing factors. *FEBS Lett*. 2013;587:417–424. doi: 10.1016/j.febslet.2013.01.035.
51. Rahaman SO, Lennon DJ, Febbraio M, Podrez EA, Hazen SL, Silverstein RL. A CD36-dependent signaling cascade is necessary for macrophage foam cell formation. *Cell Metab*. 2006;4:211–221. doi: 10.1016/j.cmet.2006.06.007.
52. Schrijvers DM, De Meyer GR, Herman AG, Martinet W. Phagocytosis in atherosclerosis: molecular mechanisms and implications for plaque progression and stability. *Cardiovasc Res*. 2007;73:470–480. doi: 10.1016/j.cardiores.2006.09.005.
53. Niazi F, Valadkhan S. Computational analysis of functional long noncoding RNAs reveals lack of peptide-coding capacity and parallels with 3' UTRs. *RNA*. 2012;18:825–843. doi: 10.1261/rna.029520.111.
54. Zhang H, Xue C, Wang Y, Shi J, Zhang X, Li W, Nunez S, Foulkes AS, Lin J, Hinkle CC, Yang W, Morrissey EE, Rader DJ, Li M, Reilly MP. Deep rna sequencing uncovers a repertoire of human macrophage long intergenic noncoding rnas modulated by macrophage activation and associated with cardiometabolic diseases. *J Am Heart Assoc*. 2017;6:e007431.

Highlights

- Diabetes mellitus upregulates long noncoding RNA *Dnm3os* (dynamin 3 opposite strand) in mouse macrophages and human monocytes.
- Diabetic conditions in vitro induce *Dnm3os* in macrophages via NF- κ B activation.
- *Dnm3os* increases inflammatory gene expression and phagocytosis in macrophages.
- Human ortholog (*DNM3OS*) is also upregulated under diabetic conditions and exhibits proinflammatory phenotype in human macrophages.
- *Dnm3os* interacts with nucleolin in macrophages and disruption of this interaction in diabetes mellitus upregulates inflammatory genes via epigenetic chromatin histone lysine acetylation.